



UNIVERSITY OF LEEDS

This is a repository copy of *Regularized MFS solution of inverse boundary value problems in three-dimensional steady-state linear thermoelasticity*.

White Rose Research Online URL for this paper:
<http://eprints.whiterose.ac.uk/96525/>

Version: Accepted Version

Article:

Marin, L, Karageorghis, A and Lesnic, D (2016) Regularized MFS solution of inverse boundary value problems in three-dimensional steady-state linear thermoelasticity. *International Journal of Solids and Structures*, 91. pp. 127-142. ISSN 0020-7683

<https://doi.org/10.1016/j.ijsolstr.2016.03.013>

© 2016. This manuscript version is made available under the CC-BY-NC-ND 4.0 license
<http://creativecommons.org/licenses/by-nc-nd/4.0/>

Reuse

Unless indicated otherwise, fulltext items are protected by copyright with all rights reserved. The copyright exception in section 29 of the Copyright, Designs and Patents Act 1988 allows the making of a single copy solely for the purpose of non-commercial research or private study within the limits of fair dealing. The publisher or other rights-holder may allow further reproduction and re-use of this version - refer to the White Rose Research Online record for this item. Where records identify the publisher as the copyright holder, users can verify any specific terms of use on the publisher's website.

Takedown

If you consider content in White Rose Research Online to be in breach of UK law, please notify us by emailing eprints@whiterose.ac.uk including the URL of the record and the reason for the withdrawal request.



eprints@whiterose.ac.uk
<https://eprints.whiterose.ac.uk/>

REGULARIZED MFS SOLUTION OF INVERSE BOUNDARY VALUE PROBLEMS IN THREE-DIMENSIONAL STEADY-STATE LINEAR THERMOELASTICITY

LIVIU MARIN^{1,2,*}, ANDREAS KARAGEORGHIS^{3,†} AND DANIEL LESNIC^{4,‡}

¹Department of Mathematics, Faculty of Mathematics and Computer Science, University of
Bucharest,

14 Academiei, 010014 Bucharest, Romania

²Institute of Solid Mechanics, Romanian Academy, 15 Constantin Mille, 010141 Bucharest, Romania

³Department of Mathematics and Statistics, University of Cyprus/Πανεπιστήμιο Κύπρου,
P.O. Box 20537, 1678 Nicosia/Λευκωσία, Cyprus/Κύπρος

⁴Department of Applied Mathematics, University of Leeds, Leeds LS2 9JT, UK

Abstract

We investigate the numerical reconstruction of the missing thermal and mechanical boundary conditions on an inaccessible part of the boundary in the case of three-dimensional linear isotropic thermoelastic materials from the knowledge of over-prescribed noisy data on the remaining accessible boundary. We employ the method of fundamental solutions (MFS) and several singular value decomposition (SVD)-based regularization methods, e.g. the Tikhonov regularization method (Tikhonov and Arsenin, 1986), the damped SVD and the truncated SVD (Hansen, 1998), whilst the regularization parameter is selected according to the discrepancy principle (Morozov, 1966), generalized cross-validation criterion (Golub et al., 1979) and Hansen's L-curve method (Hansen and O'Leary, 1993).

Keywords: Inverse boundary value problem; Three-dimensional linear thermoelasticity; Method of fundamental solutions (MFS); Singular value decomposition (SVD); Regularization.

*Corresponding author. E-mails: marin.liviu@gmail.com; liviu.marin@fmi.unibuc.ro

†E-mail: andreask@ucy.ac.cy

‡E-mail: amt51d@maths.leeds.ac.uk

1 INTRODUCTION

For forward/direct boundary value problems (BVPs) in thermoelasticity, the thermo-mechanical equilibrium equations have to be solved in a known geometry by assuming that the material constants, the heat sources and/or body forces, and the boundary and initial conditions for the mechanical and thermal fields are all known. The total or partial lack of knowledge of at least one of these conditions leads to a so-called *inverse problem*. A classical example of an inverse problem is represented by the so-called *inverse BVPs* in which the geometry of the solution domain, the thermo-mechanical material constants and the heat sources and body forces are all known, while boundary data are not available on an inaccessible part of the boundary and, instead, over-prescribed boundary conditions are provided on the remaining boundary part. It is well-known that such inverse BVPs are generally ill-posed, in the sense that their solution in general does not exist and even if it exists, it does not depend continuously on the input data. Consequently, small errors in the input data may cause large errors in the output solution and thus a special treatment of these problems is required.

Over the last decade, the MFS and various regularization methods, such as the Tikhonov regularization method (TRM) and the singular value decomposition (SVD), have been used increasingly for the numerical solution of inverse problems. For thermo-mechanical problems in solid bodies, we mention the Cauchy problem associated with the heat conduction equation (Hon and Wei, 2004, 2005; Marin, 2008), linear elasticity (Marin, 2005a; Marin and Lesnic, 2004), steady-state heat conduction in functionally graded materials (Marin, 2005b), Helmholtz-type equations (Marin, 2005c; Marin and Lesnic, 2005a), two-dimensional linear thermoelasticity (Karageorghis et al., 2014; Marin and Karageorghis, 2013b) etc. have all been successfully solved by the MFS. For further applications of the MFS to inverse problems, we refer the reader to the survey by Karageorghis et al. (2011).

The Cauchy and the general inverse BVPs in static planar thermoelasticity have been addressed by Marin and Karageorghis (2013b), and Karageorghis et al. (2014), respectively, who applied the MFS, Hansen's L-curve criterion and the numerical inversion of the normal system of equations generated by the minimisation of the zeroth-order Tikhonov functional. Recently, Marin et al. (2015) studied both the Cauchy problem and the general inverse BVP in two-dimensional linear isotropic thermoelastic solids by employing singular value decomposition (SVD)-based non-iterative regularization methods, such as the Tikhonov regularization method (TRM) (Tikhonov and Arsenin, 1986), the damped SVD (DSVD) and the truncated

SVD (TSVD) (Hansen, 1998), in conjunction with several criteria for the selection of the corresponding regularization parameter, i.e. Morozov’s discrepancy principle (DP) (Morozov, 1966), generalized cross-validation (GCV) criterion (Golub et al., 1979) and Hansen’s L-curve (LC) method (Hansen and O’Leary, 1993). In this paper we extend that analysis to three-dimensions. Although the mathematical formulation is very similar in two- and three-dimensions, the numerical implementation is obviously more involved in the latter case. The extension of the MFS from two to three dimensions is considerably simpler than the extension of other, more traditional, discretisation methods from two to three dimensions. This, in itself, is an important advantage of the MFS over more traditional discretisation methods which is due to the fact that it is both a meshless and a boundary-type method.

The paper is organised as follows: In Section 2 we formulate mathematically the inverse BVPs under investigation and present some analysis employing a particular solution of the thermoelasticity system. New three-dimensional formulae for the MFS are provided and combined with the SVD-based non-iterative regularization methods mentioned above is presented in Section 3. The accuracy and stability of the numerical results obtained using these regularization methods and selection criteria are thoroughly analysed for two examples in three dimensions in Section 4. Finally, some concluding remarks are provided in Section 5.

2 MATHEMATICAL FORMULATION AND ANALYSIS

We consider an isotropic solid which occupies a bounded domain $\Omega \subset \mathbb{R}^3$ and is characterised by the following material constants: the thermal conductivity, κ , the coefficient of linear thermal expansion, α_T , Poisson’s ratio, ν , and the shear modulus, G .

In the framework of isotropic linear thermoelasticity, the strain tensor, $\boldsymbol{\epsilon} = [\epsilon_{ij}]_{1 \leq i, j \leq 3}$, satisfies the kinematic relation

$$\boldsymbol{\epsilon}(\mathbf{x}) = \frac{1}{2} (\nabla \mathbf{u}(\mathbf{x}) + \nabla \mathbf{u}(\mathbf{x})^T), \quad \mathbf{x} \in \bar{\Omega}, \quad (1)$$

and is related to the stress tensor, $\boldsymbol{\sigma} = [\sigma_{ij}]_{1 \leq i, j \leq 3}$, by means of the following constitutive law (Nowacki, 1986)

$$\boldsymbol{\sigma}(\mathbf{x}) = 2G \left[\boldsymbol{\epsilon}(\mathbf{x}) + \frac{\nu}{1 - 2\nu} \text{tr}(\boldsymbol{\epsilon}(\mathbf{x})) \mathbf{I} \right] - \gamma T(\mathbf{x}) \mathbf{I}, \quad \mathbf{x} \in \bar{\Omega}, \quad (2a)$$

where $\mathbf{I} = [\delta_{ij}]_{1 \leq i, j \leq 3}$ is the identity matrix in \mathbb{R}^3 and

$$\gamma = 2G\alpha_T(1 + \nu)/(1 - 2\nu). \quad (2b)$$

The kinematic relation (1) combined with the constitutive law of isotropic thermoelasticity (2a) yields

$$\boldsymbol{\sigma}(\mathbf{x}) = G \left[(\nabla \mathbf{u}(\mathbf{x}) + \nabla \mathbf{u}(\mathbf{x})^\top) + \frac{2\nu}{1-2\nu} (\nabla \cdot \mathbf{u}(\mathbf{x})) \mathbf{I} \right] - \gamma T(\mathbf{x}) \mathbf{I}, \quad \mathbf{x} \in \bar{\Omega}. \quad (3)$$

In the absence of body forces, the equilibrium equations of three-dimensional isotropic linear thermoelasticity, in terms of the displacement vector and the temperature, become

$$-\nabla \cdot \boldsymbol{\sigma}(\mathbf{x}) \equiv \mathcal{L} \mathbf{u}(\mathbf{x}) + \gamma \nabla T(\mathbf{x}) = \mathbf{0} \quad \mathbf{x} \in \Omega. \quad (4)$$

Here $\mathcal{L} = (\mathcal{L}_1, \mathcal{L}_2, \mathcal{L}_3)^\top$ is the partial differential operator associated with the three-dimensional Navier-Lamé system of isotropic linear elasticity, i.e.

$$\mathcal{L} \mathbf{u}(\mathbf{x}) \equiv -G \left[\nabla \cdot (\nabla \mathbf{u}(\mathbf{x}) + \nabla \mathbf{u}(\mathbf{x})^\top) + \frac{2\nu}{1-2\nu} \nabla (\nabla \cdot \mathbf{u}(\mathbf{x})) \right], \quad \mathbf{x} \in \Omega. \quad (5)$$

In the absence of heat sources, the governing steady-state heat conduction equation becomes

$$-\kappa \nabla^2 T(\mathbf{x}) = 0, \quad \mathbf{x} \in \Omega. \quad (6)$$

We also let $\mathbf{n}(\mathbf{x})$ be the outward unit normal vector to the boundary $\partial\Omega$ of Ω , $\mathbf{q}(\mathbf{x})$ be the normal heat flux at a point $\mathbf{x} \in \partial\Omega$ defined by

$$\mathbf{q}(\mathbf{x}) \equiv -(\kappa \nabla T(\mathbf{x})) \cdot \mathbf{n}(\mathbf{x}), \quad \mathbf{x} \in \partial\Omega, \quad (7)$$

and $\mathbf{t}(\mathbf{x})$ be the traction vector at $\mathbf{x} \in \partial\Omega$ given by

$$\mathbf{t}(\mathbf{x}) \equiv \boldsymbol{\sigma}(\mathbf{x}) \mathbf{n}(\mathbf{x}), \quad \mathbf{x} \in \partial\Omega. \quad (8)$$

In many practical situations, only a part of the boundary, say $\Gamma_1 \subset \partial\Omega$, is accessible for measurements, while the remaining boundary part, $\Gamma_2 = \partial\Omega \setminus \Gamma_1$, is inaccessible and hence no boundary data is available on it. In this case, additional measurements are available on Γ_1 , thus compensating for the lack of boundary data on Γ_2 , and this corresponds to an inverse BVP.

In the sequel, we consider the following two inverse BVPs for three-dimensional steady-state isotropic linear thermoelasticity:

Problem (A): The *Cauchy problem* given by (4) and (6) and the following over-prescribed thermal and mechanical boundary conditions:

$$T(\mathbf{x}) = \tilde{T}(\mathbf{x}) \quad \text{and} \quad \mathbf{q}(\mathbf{x}) = \tilde{\mathbf{q}}(\mathbf{x}), \quad \mathbf{x} \in \Gamma_1, \quad (9a)$$

$$\mathbf{u}(\mathbf{x}) = \tilde{\mathbf{u}}(\mathbf{x}) \quad \text{and} \quad \mathbf{t}(\mathbf{x}) = \tilde{\mathbf{t}}(\mathbf{x}), \quad \mathbf{x} \in \Gamma_1. \quad (9b)$$

Problem (B): The *inverse BVP* given by (4) and (6) and the following boundary conditions:

$$T(\mathbf{x}) = \tilde{T}(\mathbf{x}), \quad \mathbf{x} \in \Gamma_1, \quad (10a)$$

$$\mathbf{u}(\mathbf{x}) = \tilde{\mathbf{u}}(\mathbf{x}), \quad \mathbf{x} \in \Gamma_1, \quad (10b)$$

$$\mathbf{t}(\mathbf{x}) = \tilde{\mathbf{t}}(\mathbf{x}), \quad \mathbf{x} \in \partial\Omega. \quad (10c)$$

In the case of the Cauchy problem (4), (6), (9a) and (9b), we can decouple the solutions for T and \mathbf{u} . Indeed, by first solving the Cauchy problem for the Laplace equation given by Eqs. (6) and (9a), we can obtain the temperature T and its gradient ∇T in Ω . Then, introducing this gradient into (4), we are left to solve the Cauchy problem for the Navier-Lamé system of isotropic linear elasticity given by Eqs. (4) and (9b). This decoupling is useful to show the uniqueness of the solution (T, \mathbf{u}) of Problem (A), but we still need to deal with solving two Cauchy problems which are ill-posed by violating the continuous dependence on the input data. In the case of the inverse BVP given by Eqs. (4), (6), (10a) and (10b), the uniqueness of the solution was proved by Kozlov et al. (2009), but the problem is still ill-posed. In order to deal with the ill-posedness of these problems, suitable regularization procedures should be employed.

3 METHOD OF FUNDAMENTAL SOLUTIONS

Nevertheless, the numerical discretisation of the thermoelasticity system of equations (4) and (6) in three-dimensional homogeneous materials can be conveniently performed using the boundary element method (BEM) as described by Rizzo and Shippy (1977). This results in advantageously having to discretise two-dimensional boundary (surface) integrals instead of three-dimensional volume integrals as it happens with domain discretisation methods such as the finite element method (FEM). However, in this study we are able to simplify the numerical implementation even further and employ instead the meshless MFS. For the coupled system (4) and (6) of steady-state linear thermoelasticity the MFS is described in the next subsections.

3.1 APPROXIMATION FOR THE THERMAL PROBLEM

The fundamental solution of the three-dimensional Laplace equation (6) is given by

$$F(\mathbf{x}, \boldsymbol{\xi}) = \frac{1}{4\pi\kappa} \frac{1}{\|\mathbf{x} - \boldsymbol{\xi}\|}, \quad (\mathbf{x}, \boldsymbol{\xi}) \in \mathbb{R}^3 \times \mathbb{R}^3. \quad (11)$$

In the MFS, the temperature is approximated by a linear combination of fundamental solutions with respect to N_L sources, $\{\boldsymbol{\xi}^{(n)}\}_{n=1, \overline{N_L}} \subset \mathbb{R}^3 \setminus \overline{\Omega}$, in the form

$$\mathbf{T}(\mathbf{x}) \approx \mathbf{T}_{N_L}(\mathbf{c}^{(1)}, \boldsymbol{\xi}; \mathbf{x}) = \sum_{n=1}^{N_L} \mathbf{F}(\mathbf{x}, \boldsymbol{\xi}^{(n)}) c_n^{(1)}, \quad \mathbf{x} \in \overline{\Omega}, \quad (12)$$

where $\mathbf{c}^{(1)} = (c_1^{(1)}, \dots, c_{N_L}^{(1)}) \in \mathbb{R}^{N_L}$ and $\boldsymbol{\xi} \in \mathbb{R}^{3N_L}$ is a vector containing the coordinates of the sources.

From Eqs. (7) and (12), it follows that the normal heat flux can be approximated by

$$\mathbf{q}(\mathbf{x}) \approx \mathbf{q}_{N_L}(\mathbf{c}^{(1)}, \boldsymbol{\xi}; \mathbf{x}) = \frac{1}{4\pi} \sum_{n=1}^{N_L} \frac{(\mathbf{x} - \boldsymbol{\xi}^{(n)}) \cdot \mathbf{n}(\mathbf{x})}{\|\mathbf{x} - \boldsymbol{\xi}^{(n)}\|^3} c_n^{(1)}, \quad \mathbf{x} \in \partial\Omega. \quad (13)$$

Next, we select M_L^1 collocation points, $\{\mathbf{x}^{(n)}\}_{n=1, \overline{M_L^1}}$, on the boundary Γ_1 and M_L^2 collocation points, $\{\mathbf{x}^{(M_L^1+n)}\}_{n=1, \overline{M_L^2}}$, on the boundary Γ_2 , such that $M_L^1 + M_L^2 = M_L$. By collocating the thermal boundary conditions (9a) or (10a), one obtains the following linear system of equations for the unknown coefficients $\mathbf{c}^{(1)} \in \mathbb{R}^{N_L}$:

$$\mathbf{A}^{(11)} \mathbf{c}^{(1)} = \mathbf{f}^{(1)}. \quad (14)$$

Here $\mathbf{A}^{(11)}$ is the MFS matrix associated with the thermal part of the inverse problem under investigation and $\mathbf{f}^{(1)}$ contains the corresponding discretised thermal data. More precisely, the dimensions of $\mathbf{A}^{(11)}$ and $\mathbf{f}^{(1)}$ are given by

- (i) $\mathbf{A}^{(11)} \in \mathbb{R}^{2M_L^1 \times N_L}$ and $\mathbf{f}^{(1)} \in \mathbb{R}^{2M_L^1}$ for Problem (A);
- (ii) $\mathbf{A}^{(11)} \in \mathbb{R}^{M_L^1 \times N_L}$ and $\mathbf{f}^{(1)} \in \mathbb{R}^{M_L^1}$ for Problem (B).

Next, we seek the displacement \mathbf{u} as a superposition, see Marin and Karageorghis (2013a),

$$\mathbf{u} = \mathbf{u}^{(H)} + \mathbf{u}^{(P)}, \quad (15)$$

where $\mathbf{u}^{(P)}$ is a particular solution of the non-homogeneous system (4) and $\mathbf{u}^{(H)}$ is the solution of the homogeneous problem

$$\mathcal{L}\mathbf{u}^{(H)}(\mathbf{x}) = \mathbf{0}, \quad \mathbf{x} \in \Omega, \quad (16a)$$

$$\mathbf{u}^{(H)}(\mathbf{x}) = \tilde{\mathbf{u}}(\mathbf{x}) - \mathbf{u}^{(P)}(\mathbf{x}), \quad \mathbf{x} \in \Gamma_1, \quad (16b)$$

$$\mathbf{t}^{(H)}(\mathbf{x}) = \tilde{\mathbf{t}}(\mathbf{x}) - \mathbf{t}^{(P)}(\mathbf{x}), \quad \mathbf{x} \in \partial\Omega. \quad (16c)$$

3.2 APPROXIMATION FOR THE NON-HOMOGENEOUS EQUILIBRIUM EQUATIONS (4)

A particular solution to the non-homogeneous equilibrium equations (4) in \mathbb{R}^3 is given by, see e.g. Karageorghis and Smyrlis (2007),

$$\mathbf{u}^{(P)}(\mathbf{y}) \approx \mathbf{u}_{N_L}^{(P)}(\mathbf{c}^{(1)}, \boldsymbol{\xi}; \mathbf{y}) = \frac{\alpha_T}{2} \left(\frac{1+\nu}{1-\nu} \right) \sum_{n=1}^{N_L} F(\mathbf{y}, \boldsymbol{\xi}^{(n)}) (\mathbf{y} - \boldsymbol{\xi}^{(n)}) c_n^{(1)}, \quad \mathbf{y} \in \mathbb{R}^3 \setminus \bigcup_{n=1}^{N_L} \{\boldsymbol{\xi}^{(n)}\}. \quad (17)$$

The corresponding approximation for the particular traction vector is given by

$$\begin{aligned} \mathbf{t}^{(P)}(\mathbf{y}) \approx & -\frac{\alpha_T G}{4\pi\kappa} \left(\frac{1+\nu}{1-\nu} \right) \sum_{n=1}^{N_L} \left[-\frac{1}{1-2\nu} \frac{1}{\|\mathbf{y} - \boldsymbol{\xi}^{(n)}\|} \mathbf{n}(\mathbf{y}) \right. \\ & \left. + \frac{(\mathbf{y} - \boldsymbol{\xi}^{(n)}) \cdot \mathbf{n}(\mathbf{y})}{\|\mathbf{y} - \boldsymbol{\xi}^{(n)}\|^3} (\mathbf{y} - \boldsymbol{\xi}^{(n)}) \right] c_n^{(1)}, \quad \mathbf{y} \in \partial\Omega. \end{aligned} \quad (18)$$

3.3 APPROXIMATION FOR THE HOMOGENEOUS MECHANICAL PROBLEM

The fundamental solution matrix $\mathbf{U} = [\mathbf{U}_{ij}]_{1 \leq i, j \leq 3}$ for the displacement vector in three-dimensional isotropic linear elasticity is given by (Aliabadi, 2002)

$$\begin{aligned} \mathbf{U}_{ij}(\mathbf{y}, \boldsymbol{\eta}) = & \frac{1}{16\pi G(1-\nu)} \frac{1}{\|\mathbf{y} - \boldsymbol{\eta}\|} \left[(3-4\nu) \delta_{ij} + \frac{y_i - \eta_i}{\|\mathbf{y} - \boldsymbol{\eta}\|} \frac{y_j - \eta_j}{\|\mathbf{y} - \boldsymbol{\eta}\|} \right], \\ & (\mathbf{y}, \boldsymbol{\eta}) \in \mathbb{R}^3 \times \mathbb{R}^3, \quad i, j = 1, 2, 3. \end{aligned} \quad (19)$$

By differentiating Eq. (19) with respect to y_k , $k = 1, 2, 3$, one obtains the derivatives of the fundamental solution for the displacement vector, denoted by $\partial_{y_k} \mathbf{U}_{ij}(\mathbf{y}, \boldsymbol{\eta})$, where $\partial_{y_k} \equiv \partial / \partial y_k$. The fundamental solution matrix $\mathbf{T} = [\mathbf{T}_{ij}]_{1 \leq i, j \leq 3}$ for the traction vector in the case of three-dimensional isotropic linear elasticity is then obtained by combining equation (19) with the definition of the traction vector (8) and Hooke's constitutive law of isotropic linear elasticity (Aliabadi, 2002), namely

$$\begin{aligned} \mathbf{T}_{1k}(\mathbf{y}, \boldsymbol{\eta}) = & \frac{2G}{1-2\nu} \left[(1-\nu) \partial_{y_1} \mathbf{U}_{1k}(\mathbf{y}, \boldsymbol{\eta}) + \nu (\partial_{y_2} \mathbf{U}_{2k}(\mathbf{y}, \boldsymbol{\eta}) + \partial_{y_3} \mathbf{U}_{3k}(\mathbf{y}, \boldsymbol{\eta})) \right] \mathbf{n}_1(\mathbf{y}) \\ & + G \left[\partial_{y_2} \mathbf{U}_{1k}(\mathbf{y}, \boldsymbol{\eta}) + \partial_{y_1} \mathbf{U}_{2k}(\mathbf{y}, \boldsymbol{\eta}) \right] \mathbf{n}_2(\mathbf{y}) + G \left[\partial_{y_3} \mathbf{U}_{1k}(\mathbf{y}, \boldsymbol{\eta}) + \partial_{y_1} \mathbf{U}_{3k}(\mathbf{y}, \boldsymbol{\eta}) \right] \mathbf{n}_3(\mathbf{y}), \end{aligned} \quad (20a)$$

$$k = 1, 2, 3,$$

$$\begin{aligned} \mathbf{T}_{2k}(\mathbf{y}, \boldsymbol{\eta}) = & \frac{2G}{1-2\nu} \left[(1-\nu) \partial_{y_2} \mathbf{U}_{2k}(\mathbf{y}, \boldsymbol{\eta}) + \nu (\partial_{y_3} \mathbf{U}_{3k}(\mathbf{y}, \boldsymbol{\eta}) + \partial_{y_1} \mathbf{U}_{1k}(\mathbf{y}, \boldsymbol{\eta})) \right] \mathbf{n}_2(\mathbf{y}) \\ & + G \left[\partial_{y_3} \mathbf{U}_{2k}(\mathbf{y}, \boldsymbol{\eta}) + \partial_{y_2} \mathbf{U}_{3k}(\mathbf{y}, \boldsymbol{\eta}) \right] \mathbf{n}_3(\mathbf{y}) + G \left[\partial_{y_1} \mathbf{U}_{2k}(\mathbf{y}, \boldsymbol{\eta}) + \partial_{y_2} \mathbf{U}_{1k}(\mathbf{y}, \boldsymbol{\eta}) \right] \mathbf{n}_1(\mathbf{y}), \end{aligned} \quad (20b)$$

$$k = 1, 2, 3,$$

and

$$\begin{aligned} \mathbf{T}_{3k}(\mathbf{y}, \boldsymbol{\eta}) &= \frac{2G}{1-2\nu} \left[(1-\nu) \partial_{y_3} \mathbf{U}_{3k}(\mathbf{y}, \boldsymbol{\eta}) + \nu (\partial_{y_1} \mathbf{U}_{1k}(\mathbf{y}, \boldsymbol{\eta}) + \partial_{y_2} \mathbf{U}_{2k}(\mathbf{y}, \boldsymbol{\eta})) \right] \mathbf{n}_3(\mathbf{y}) \\ &+ G \left[\partial_{y_1} \mathbf{U}_{3k}(\mathbf{y}, \boldsymbol{\eta}) + \partial_{y_3} \mathbf{U}_{1k}(\mathbf{y}, \boldsymbol{\eta}) \right] \mathbf{n}_1(\mathbf{y}) + G \left[\partial_{y_2} \mathbf{U}_{3k}(\mathbf{y}, \boldsymbol{\eta}) + \partial_{y_3} \mathbf{U}_{2k}(\mathbf{y}, \boldsymbol{\eta}) \right] \mathbf{n}_2(\mathbf{y}), \end{aligned} \quad (20c)$$

$$k = 1, 2, 3.$$

As for the thermal problem, we consider N_E sources, $\{\boldsymbol{\eta}^{(n)}\}_{n=\overline{1, N_E}}$, and approximate the displacement vector, $\mathbf{u}^{(H)}$, associated with the homogeneous equilibrium equation (16a) by a linear combination of the displacement fundamental solutions (19) with respect to these sources, i.e.

$$\mathbf{u}^{(H)}(\mathbf{y}) \approx \mathbf{u}_{N_E}^{(H)}(\mathbf{c}^{(2)}, \boldsymbol{\eta}; \mathbf{y}) = \sum_{n=1}^{N_E} \mathbf{U}(\mathbf{y}, \boldsymbol{\eta}^{(n)}) \mathbf{c}_n^{(2)}, \quad \mathbf{y} \in \overline{\Omega}, \quad (21)$$

where $\mathbf{c}_n^{(2)} \in \mathbb{R}^3$, $n = \overline{1, N_E}$, $\mathbf{c}^{(2)} = (\mathbf{c}_1^{(2)}, \mathbf{c}_2^{(2)}, \dots, \mathbf{c}_{N_E}^{(2)}) \in \mathbb{R}^{3N_E}$ and $\boldsymbol{\eta} \in \mathbb{R}^{3N_E}$ is a vector containing the coordinates of the sources $\{\boldsymbol{\eta}^{(n)}\}_{n=\overline{1, N_E}}$. In a similar manner, the traction vector, $\mathbf{t}^{(H)}$, associated with the homogeneous equilibrium equation (16a) is approximated by a linear combination of the traction fundamental solutions (20a)–(20c), namely

$$\mathbf{t}^{(H)}(\mathbf{y}) \approx \mathbf{t}_{N_E}^{(H)}(\mathbf{c}^{(2)}, \boldsymbol{\eta}; \mathbf{y}) = \sum_{n=1}^{N_E} \mathbf{T}(\mathbf{y}, \boldsymbol{\eta}^{(n)}) \mathbf{c}_n^{(2)}, \quad \mathbf{y} \in \partial\Omega. \quad (22)$$

By collocating the corresponding boundary conditions (16b) and (16c) at the points $\{\mathbf{y}^{(n)}\}_{n=\overline{1, M_E^1}}$ on the boundary portion Γ_1 and, eventually, $\{\mathbf{y}^{(M_E^1+n)}\}_{n=\overline{1, M_E^2}}$ on the boundary portion Γ_2 , one obtains the following linear system of equations for the unknown coefficients $\mathbf{c}^{(2)} \in \mathbb{R}^{3N_E}$:

$$\mathbf{A}^{(22)} \mathbf{c}^{(2)} = \mathbf{f}^{(2)} - \mathbf{A}^{(21)} \mathbf{c}^{(1)}. \quad (23)$$

Here $\mathbf{A}^{(22)}$ is the MFS matrix associated with the homogeneous mechanical part of the inverse problem under investigation, $\mathbf{f}^{(2)}$ is the right-hand side vector containing the corresponding discretised mechanical data available on Γ_1 and, eventually, Γ_2 . The matrix $\mathbf{A}^{(21)}$ represents the coupling of the mechanical part of the inverse problem considered with its thermal part (more specifically, the influence of the thermal field on the mechanical field). More precisely, the dimensions of $\mathbf{A}^{(21)}$, $\mathbf{A}^{(22)}$ and $\mathbf{f}^{(2)}$ are given by:

- (i) $\mathbf{A}^{(21)} \in \mathbb{R}^{6M_E^1 \times N_L}$, $\mathbf{A}^{(22)} \in \mathbb{R}^{6M_E^1 \times 3N_E}$ and $\mathbf{f}^{(2)} \in \mathbb{R}^{6M_E^1}$ for Problem (A);
- (ii) $\mathbf{A}^{(21)} \in \mathbb{R}^{(6M_E^1 + 3M_E^2) \times N_L}$, $\mathbf{A}^{(22)} \in \mathbb{R}^{(6M_E^1 + 3M_E^2) \times 3N_E}$ and $\mathbf{f}^{(2)} \in \mathbb{R}^{6M_E^1 + 3M_E^2}$ for Problem (B).

3.4 REGULARIZATION OF THE INVERSE THERMOELASTICITY PROBLEMS

From Eqs. (14) and (23), it follows that the MFS formulation for both inverse problems (A) and (B) may be recast as

$$\mathbf{A} \mathbf{c} = \mathbf{f}. \quad (24a)$$

The matrix $\mathbf{A} \in \mathbb{R}^{m \times n}$ and the vectors $\mathbf{c} \in \mathbb{R}^n$ and $\mathbf{f} \in \mathbb{R}^m$ in (24a), where $m = 2M_L^1 + 6M_E^1$ and $n = N_L + 3N_E$, and $m = M_L^1 + 6M_E^1 + 3M_E^2$ and $n = N_L + 3N_E$ for inverse problems (A) and (B), respectively, are given by

$$\mathbf{A} = \begin{bmatrix} \mathbf{A}^{(11)} & \mathbf{0} \\ \mathbf{A}^{(21)} & \mathbf{A}^{(22)} \end{bmatrix}, \quad \mathbf{c} = \begin{pmatrix} \mathbf{c}^{(1)} \\ \mathbf{c}^{(2)} \end{pmatrix}, \quad \mathbf{f} = \begin{pmatrix} \mathbf{f}^{(1)} \\ \mathbf{f}^{(2)} \end{pmatrix}. \quad (24b)$$

Clearly, once the MFS coefficients $\mathbf{c}^{(1)} \in \mathbb{R}^{N_L}$ and $\mathbf{c}^{(2)} \in \mathbb{R}^{3N_E}$ have been determined accurately, the approximations for the unknown temperature and displacement are obtained using the superposition principle together with Eqs. (15), (17), (18) and (22).

In order to uniquely determine the solution $\mathbf{c} \in \mathbb{R}^{N_L+3N_E}$ of the system of equations (24a), the numbers of boundary collocation points and sources must satisfy the inequality $2M_L^1 + 6M_E^1 \geq N_L + 3N_E$ for inverse problem (A), or $M_L^1 + 6M_E^1 + 3M_E^2 \geq N_L + 3N_E$ for inverse problem (B). In practice, the same collocation points and sources are used for both the thermal and the mechanical problems, i.e. $\{\mathbf{x}^{(m)}\}_{m=1, \overline{M_L}} = \{\mathbf{y}^{(m)}\}_{m=1, \overline{M_E}}$ with $M_L = M_E =: M$ and $\{\boldsymbol{\xi}^{(n)}\}_{n=1, \overline{N_L}} = \{\boldsymbol{\eta}^{(n)}\}_{n=1, \overline{N_E}}$ with $N_L = N_E =: N$, respectively. Consequently, the inequality that ensures the uniqueness of the solution of the system of equations (24a) reduces to $2M_1 \geq N$ for inverse problem (A), or $M_1 + 3M/4 \geq N$ for inverse problem (B), where $M_j := M_L^j = M_E^j$, $j = 1, 2$.

Since inverse problems (A) and (B) are ill-posed, the system of equations (24a) is ill-conditioned and needs to be regularized. For this purpose, we compare several regularization methods such as:

(R1) the Tikhonov regularization method (TRM);

(R2) the damped SVD (DSVD);

(R3) the truncated SVD (TSVD);

with the choice of the regularization parameter given by

(C1) the L-curve criterion (LC);

(C2) the discrepancy principle (DP);

(C3) the generalized cross-validation (GCV).

The full description of these methods and criteria for selecting the regularization parameter λ for the TRM and DSVD and truncation number k for the TSVD can be found in Marin et al. (2015).

4 NUMERICAL RESULTS

In this section, we apply the regularized MFS described in Section 3 to two test problems. More precisely, we solve the inverse problems (A) and (B) in three-dimensional simply connected domains with smooth or piecewise smooth boundaries, for an isotropic linear thermoelastic material (copper alloy) characterised by the material constants $G = 4.80 \times 10^{10} \text{ N/m}^2$, $\nu = 0.34$, $\kappa = 4.01 \text{ W m}^{-1} \text{ K}^{-1}$ and $\alpha_T = 16.5 \times 10^{-6} \text{ }^\circ\text{C}^{-1}$.

Example 1 (Simply connected domain with a piecewise smooth boundary): We consider the inverse Cauchy problem (A) in the cube $\Omega = (-0.5, 0.5)^3$, with the analytical solution given by

$$\mathbf{T}(\mathbf{x}) = \sum_{k=1}^K \frac{\mathbf{T}_k}{\|\mathbf{x} - \mathbf{x}^{(k)}\|}, \quad \mathbf{x} \in \bar{\Omega}, \quad (25a)$$

$$\mathbf{u}(\mathbf{x}) = \frac{\gamma}{4G} \left(\frac{1-2\nu}{1-\nu} \right) \sum_{k=1}^K \mathbf{T}_k \frac{\mathbf{x} - \mathbf{x}^{(k)}}{\|\mathbf{x} - \mathbf{x}^{(k)}\|}, \quad \mathbf{x} \in \bar{\Omega}, \quad (25b)$$

$$q(\mathbf{x}) = -\kappa \sum_{k=1}^K \mathbf{T}_k \frac{(\mathbf{x} - \mathbf{x}^{(k)}) \cdot \mathbf{n}(\mathbf{x})}{\|\mathbf{x} - \mathbf{x}^{(k)}\|^3}, \quad \mathbf{x} \in \partial\Omega, \quad (25c)$$

$$\begin{aligned} \mathbf{t}(\mathbf{x}) = & -\frac{\gamma}{2} \left(\frac{1-2\nu}{1-\nu} \right) \sum_{k=1}^K \frac{\mathbf{T}_k}{\|\mathbf{x} - \mathbf{x}^{(k)}\|} \left[\mathbf{n}(\mathbf{x}) + \frac{(\mathbf{x} - \mathbf{x}^{(k)}) \cdot \mathbf{n}(\mathbf{x})}{\|\mathbf{x} - \mathbf{x}^{(k)}\|^2} (\mathbf{x} - \mathbf{x}^{(k)}) \right] \\ & - \gamma \mathbf{n}(\mathbf{x}) \sum_{k=1}^K \frac{\mathbf{T}_k}{\|\mathbf{x} - \mathbf{x}^{(k)}\|}, \quad \mathbf{x} \in \partial\Omega, \end{aligned} \quad (25d)$$

with $K = 2$, $\mathbf{x}^{(1)} = (-5.0, -5.0, 5.0)$, $\mathbf{T}_1 = -1.000^\circ\text{C}$, $\mathbf{x}^{(2)} = (2.0, -4.0, 4.0)$ and $\mathbf{T}_2 = 200^\circ\text{C}$. Clearly, the analytical solutions (25a)–(25b) satisfy the thermoelasticity system of equations (4) and (6) because they are just superpositions of *non-singular fundamental solutions*, as in the MFS expansions (12) and (17). Although they appear simple in form, they in fact are severe test examples because expressions (25a)–(25b) cannot be analytically continued to the whole of

\mathbb{R}^3 , since they possess singularities at $\mathbf{x}^{(1)}$ and $\mathbf{x}^{(2)}$. This in turn places some restrictions on the placement of the fictitious boundary $\partial\tilde{\Omega}$, enclosing the solution domain Ω , can be located, as $\tilde{\Omega}$ cannot contain the singularity points $\mathbf{x}^{(1)}$ and $\mathbf{x}^{(2)}$. For Example 1, we consider three cases, namely

(a) Over-determined Cauchy data, i.e.

$$\begin{aligned}\Gamma_1 &= \{\mathbf{x} \in \partial\Omega \mid x_1 = \pm 0.5\} \cup \{\mathbf{x} \in \partial\Omega \mid x_2 = -0.5\} \cup \{\mathbf{x} \in \partial\Omega \mid x_3 = -0.5\}; \\ \Gamma_2 &= \{\mathbf{x} \in \partial\Omega \mid x_2 = 0.5\} \cup \{\mathbf{x} \in \partial\Omega \mid x_3 = 0.5\}.\end{aligned}$$

(b) Equally determined Cauchy data, i.e.

$$\begin{aligned}\Gamma_1 &= \{\mathbf{x} \in \partial\Omega \mid x_1 = -0.5\} \cup \{\mathbf{x} \in \partial\Omega \mid x_2 = -0.5\} \cup \{\mathbf{x} \in \partial\Omega \mid x_3 = -0.5\}; \\ \Gamma_2 &= \{\mathbf{x} \in \partial\Omega \mid x_1 = 0.5\} \cup \{\mathbf{x} \in \partial\Omega \mid x_2 = 0.5\} \cup \{\mathbf{x} \in \partial\Omega \mid x_3 = 0.5\}.\end{aligned}$$

(c) Under-determined Cauchy data, i.e.

$$\begin{aligned}\Gamma_1 &= \{\mathbf{x} \in \partial\Omega \mid x_1 = -0.5\} \cup \{\mathbf{x} \in \partial\Omega \mid x_2 = -0.5\}; \\ \Gamma_2 &= \{\mathbf{x} \in \partial\Omega \mid x_1 = 0.5\} \cup \{\mathbf{x} \in \partial\Omega \mid x_2 = 0.5\} \cup \{\mathbf{x} \in \partial\Omega \mid x_3 = \pm 0.5\}.\end{aligned}$$

Example 2 (Simply connected domain with a smooth boundary): We consider the inverse BVP (B) in the sphere $\Omega = \{\mathbf{x} \in \mathbb{R}^3 \mid \|\mathbf{x}\| < R\}$, $R = 1.0$, with the analytical solution given by Eqs. (25a)–(25d), with $K = 2$, $\mathbf{x}^{(1)} = (5.0, 5.0, 5.0)$, $T_1 = 2.000^\circ\text{C}$, $\mathbf{x}^{(2)} = (-2.0, 4.0, 4.0)$ and $T_2 = -500^\circ\text{C}$. Here, we consider $\Gamma_1 = \{\mathbf{x} \in \partial\Omega \mid \rho(\mathbf{x}) = R, \theta(\mathbf{x}) \in [0, 2\pi), \phi(\mathbf{x}) \in [0, \phi_0]\}$, where $\phi_0 \in \{\pi/2, 2\pi/3\}$ and $(\rho(\mathbf{x}), \theta(\mathbf{x}), \phi(\mathbf{x}))$ are the spherical coordinates associated with $\mathbf{x} \in \mathbb{R}^3$, whilst $\Gamma_2 = \partial\Omega \setminus \Gamma_1$.

At this stage, it is worth mentioning that although Examples 1 and 2 are formulated in simple three-dimensional geometries such as a cube or a sphere, the MFS may be applied in almost exactly the same way to any other arbitrary and irregular domains as the data preparation required and the implementational details involved are similar. In fact, this is one of the important advantages that the MFS has over other discretisation methods. This advantage is, clearly, even more pronounced in (higher) three-dimensions.

In all examples we took $M_L^j = M_E^j = M_j$ uniformly distributed collocation points on Γ_j , $j = 1, 2$, such that $M_1 + M_2 = M$. Also, we took $N_L = N_E = N$ uniformly distributed sources

associated with both the over- and under-specified boundaries Γ_1 and Γ_2 , respectively. Moreover, the sources are preassigned and kept fixed throughout the solution process (i.e. the so-called static MFS approach has been employed) on a pseudo-boundary $\partial\tilde{\Omega}$ of a similar shape to that of $\partial\Omega$ such that $\text{dist}(\partial\tilde{\Omega}, \partial\Omega)$ is a fixed constant (Gorzelańczyk and Kołodziej, 2008). According to the notation used in Section 3, the corresponding MFS parameters have been set as follows:

- (i) **Example 1:** $N = 486$ on $\partial\tilde{\Omega}$, where $\tilde{\Omega} = (-0.5 - d, 0.5 + d)^3$ and $d = 4.0$, and $M_1 = \ell N/6$ on Γ_1 , with $\ell \in \{4, 3, 2\}$ corresponding to cases (a)–(c), respectively.
- (ii) **Example 2:** $N = 840$ on $\partial\tilde{\Omega} = \{\mathbf{x} \in \mathbb{R}^3 \mid \|\mathbf{x}\| = R + d\}$, where $d = 4.0$ and $M = (\phi_0/\pi)N$ on Γ_1 , for $\phi_0 \in \{\pi/2, 2\pi/3\}$.

In order to simulate the inherent measurement errors, we consider that the boundary data corresponding to the inverse problems investigated herein is noisy. More precisely, we assume that the given exact boundary data $\tilde{F}|_{\Gamma_1} = F^{(\text{an})}|_{\Gamma_1}$ or, eventually, $\tilde{F}|_{\partial\Omega} = F^{(\text{an})}|_{\partial\Omega}$ has been perturbed as

$$\tilde{F}^\varepsilon(\mathbf{x}) = (1 + p_F \zeta) F^{(\text{an})}(\mathbf{x}), \quad \mathbf{x} \in \Gamma, \quad (26)$$

where $\Gamma = \Gamma_1$ or $\Gamma = \partial\Omega$, p_F is the percentage noise and ζ is a pseudo-random number drawn from the standard uniform distribution on the interval $[-1, 1]$ generated using the `MATLAB`[®] command `-1 + 2 * rand(·)`. It should be mentioned that, for the inverse problems with noisy boundary data considered, the accuracy of the numerical results was found to be quite insensitive with respect to the location of the MFS pseudo-boundary. For all examples considered, the L-curves, the DP curves and the GCV functions, as well as the calculation of the corresponding values of the regularization parameters, were carried out using the `MATLAB`[®] routines available in Hansen’s regularization tools package (Hansen, 1994, 2007).

Further, to assess the accuracy and convergence of the combined MFS-MPS approach and SVD-based regularizing methods (R1)–(R3) in conjunction with the selection criteria (C1)–(C3), for any real-valued function $f : \Gamma \rightarrow \mathbb{R}$, where $\Gamma = \Gamma_2$ or $\Gamma = \partial\Omega$, and any set of points $\{\mathbf{x}^{(n)}\}_{n=1, \dots, N_\Gamma} \subset \Gamma$, we introduce the following *relative root mean square (RMS) error* of f on Γ :

$$e_\Gamma(f) = \sqrt{\frac{1}{N_\Gamma} \sum_{n=1}^{N_\Gamma} [f^{(\text{num})}(\mathbf{x}^{(n)}) - f(\mathbf{x}^{(n)})]^2} \bigg/ \sqrt{\frac{1}{N_\Gamma} \sum_{n=1}^{N_\Gamma} f(\mathbf{x}^{(n)})^2}, \quad (27a)$$

where $f^{(\text{num})}(\mathbf{x})$ denotes an approximate numerical value for $f(\mathbf{x})$, $\mathbf{x} \in \Gamma$. To investigate the local accuracy of the numerical solution, one could also employ the following *pointwise normalized*

error of f at $\mathbf{x} \in \Gamma$:

$$E_f(\mathbf{x}) = \frac{|f^{(\text{num})}(\mathbf{x}) - f(\mathbf{x})|}{\max_{\mathbf{y} \in \Gamma} |f(\mathbf{y})|}, \quad \mathbf{x} \in \Gamma. \quad (27b)$$

Tables 1–3 present the values of the regularization parameter λ or the truncation number k and the corresponding RMS errors, $e_{\Gamma_2}(\mathbf{T})$, $e_{\Gamma_2}(\mathbf{q})$, $e_{\Gamma_2}(\mathbf{u})$ and $e_{\Gamma_2}(\mathbf{t})$, obtained using the non-iterative regularization methods (R1)–(R3), the criteria (C1)–(C3) and various amounts of noise added to the data (9a)–(9b), for Example 1 with $|\Gamma_1|/|\Gamma_2| \in \{2, 1, 1/2\}$, i.e. cases (a)–(c), respectively. It can be observed from these tables that each of the regularization methods (R1)–(R3) has a stabilising/regularizing effect on the numerical solution of Cauchy problem (A), provided that an appropriate criterion is employed for the selection of the regularization parameter λ or the truncation number k , for over-, equally- and under-determined Cauchy data. More precisely, all of the criteria (C1)–(C3) are suitable criteria for the regularization methods (R1)–(R3).

In Figures 1 and 2 we present the numerical results retrieved in case of Example 1 with $|\Gamma_1|/|\Gamma_2| = 1$, i.e. case (b), using the TRM-LC approach and various levels of noise in the Dirichlet data $\mathbf{T}|_{\Gamma_1}$ and $\mathbf{u}|_{\Gamma_1}$, for the unknown thermal boundary data (i.e. $\mathbf{T}|_{x_2=0.5}$ and $\mathbf{q}|_{x_2=0.5}$), in comparison with their corresponding exact values. The exact and the numerical results obtained for the unknown mechanical boundary data (i.e. $\mathbf{u}_1|_{x_3=0.5}$ and $\mathbf{t}_2|_{x_3=0.5}$) are displayed in Figures 3 and 4. From Figures 1–4, as well as Tables 1–3, one can conclude that, for Example 1, very accurate and stable numerical solutions are obtained if all three regularization methods (R1)–(R3) are combined with any of the criteria (C1)–(C3), for over-, equally- and under-determined Cauchy data.

Next, we investigate the influence of the length of the over-specified boundary segment Γ_1 on the accuracy of the numerical solutions retrieved using the non-iterative regularization methods (R1)–(R3), the criteria (C1)–(C3) and various amounts of noise added to the data (9a)–(9b), for Example 1. To do so, we set $N = 486$, $d = 4$ and $p_{\mathbf{T}} = p_{\mathbf{u}} = 5\%$, and vary $M_1 = \ell N/6$ on Γ_1 , with $\ell \in \{4, 3, 2\}$ corresponding to cases (a)–(c), respectively. The exact and numerical approximations retrieved using the TSVD–DP approach and $|\Gamma_1|/|\Gamma_2| \in \{1/2, 1, 2\}$, for the temperature $\mathbf{T}|_{x_2=0.5}$, normal heat flux $\mathbf{q}|_{x_2=0.5}$, displacement $\mathbf{u}_1|_{x_3=0.5}$ and traction $\mathbf{t}_2|_{x_3=0.5}$ are presented in Figures 1–4, respectively. From these figures it can be observed that, as expected, the numerically reconstructed thermal and mechanical boundary data on Γ_2 become more inaccurate as the value of the ratio $|\Gamma_1|/|\Gamma_2|$ decreases, i.e. the surface of the boundary part Γ_1 on

which Cauchy measurements are available decreases.

Each of the regularization methods (R1)–(R3) has also a stabilising/regularizing effect on the numerical solution of Problem (B) in a three-dimensional simply connected domain with a smooth boundary, such as the sphere considered in Example 2, provided that an appropriate criterion is employed for the selection of the regularization parameter λ or the truncation number k . This can be seen from Table 4, which displays the values of the regularization parameter and the corresponding RMS errors, $e_{\Gamma_2}(\mathbf{T})$, $e_{\partial\Omega}(\mathbf{q})$ and $e_{\Gamma_2}(\mathbf{u})$, obtained using the regularization methods (R1)–(R3), the criteria (C1)–(C3) and various amounts of noise added to the data (10a)–(10c), for Example 2 with $|\Gamma_1|/|\Gamma_2| = 2$, i.e. $\phi_0 = 2\pi/3$. More precisely, all of the criteria (C1)–(C3) are suitable criteria for both the TRM and the DSVD, whilst the same conclusion holds if the TSVD is employed together with the DP only, i.e. both the LC and the GCV fail to provide a good value for k when the TSVD is used as regularization method for the inverse BVP (B) given by Example 2 with $|\Gamma_1|/|\Gamma_2| = 2$.

Figures 9 and 10 display the numerical results retrieved in case of Example 2 with $|\Gamma_1|/|\Gamma_2| = 2$ (i.e. $\phi_0 = 2\pi/3$), using the DSVD-DP approach and various levels of noise in $\mathbf{T}|_{\Gamma_1}$, $\mathbf{u}|_{\Gamma_1}$ and $\mathbf{t}|_{\partial\Omega}$, for the unknown thermal (i.e. $\mathbf{T}|_{\Gamma_2}$ and $\mathbf{q}|_{\partial\Omega}$) and the mechanical boundary data (i.e. $\mathbf{u}_1|_{\Gamma_2}$), respectively, in terms of their corresponding pointwise normalized errors (27b). From these figures, as well as Table 4, one can conclude that the numerical solutions obtained using the DSVD-DP are all very accurate and stable with respect to decreasing the amount of noise in the data, for Example 2 with $|\Gamma_1|/|\Gamma_2| = 2$.

In Table 5 we present the values of the regularization parameter and the corresponding RMS errors, $e_{\Gamma_2}(\mathbf{T})$, $e_{\partial\Omega}(\mathbf{q})$ and $e_{\Gamma_2}(\mathbf{u})$, obtained using the regularization methods (R1)–(R3), the criteria (C1)–(C3) and various amounts of noise added to the data (9a)–(9b), for Example 2 with $|\Gamma_1|/|\Gamma_2| = 1$, i.e. $\phi_0 = \pi/2$. From this table we see that each of the regularization methods (R1)–(R3) has a stabilising/regularizing effect on the numerical solution of Example 2 with $|\Gamma_1|/|\Gamma_2| = 1$, provided that an appropriate criterion is employed for the selection of the regularization parameter λ or the truncation number k . More precisely, both the DP and the LC are suitable criteria for all of the regularization methods (R1)–(R3), whilst the GCV fails to provide a good value for λ or k for all regularization methods in the case of Example 2 with $|\Gamma_1|/|\Gamma_2| = 1$. Also, by comparing Tables 4 and 5, one can conclude that, as expected, the smaller the boundary Γ_2 of the solution domain on which over-determined data are available, the more inaccurate the numerical reconstruction of the unknown boundary data.

Finally, we investigate the sensitivity of the numerical results obtained using the regularization methods (R1)–(R3), together with the criteria (C1)–(C3) for selecting the optimal value of the regularization parameter, with respect to the distance between the boundary $\partial\Omega$ and the pseudo-boundary $\partial\tilde{\Omega}$ on which the singularities are located, i.e. $d = \text{dist}(\partial\tilde{\Omega}, \partial\Omega)$. We consider the BVP given by Example 1 case (b), set $N = 486$ singularities on $\partial\tilde{\Omega} = \{\mathbf{x} \in \mathbb{R}^3 \mid \|\mathbf{x}\| = R+d\}$, $M = N/2$ collocation points on Γ_1 and $p_T = p_{\mathbf{u}} = 3\%$, and vary $d \in (0, 10]$. Figures 11(a)–11(c) present the accuracy errors $e_{\Gamma_2}(T)$, $e_{\Gamma_2}(q)$, $e_{\Gamma_2}(\mathbf{u})$ and $e_{\Gamma_2}(\mathbf{t})$ as functions of the distance d , obtained using the TRM-LC, DSVD-LC and TSVD-DP, respectively. From these figures it can be seen that, as expected, all the errors decrease until d reaches a threshold value, after which they stabilise reaching a plateau region.

5 CONCLUSIONS

In this paper, we have investigated the reconstruction of the missing thermal and mechanical data on an inaccessible part of the boundary for three-dimensional linear isotropic thermoelastic materials from over-prescribed noisy measurements taken on the remaining accessible boundary part. Two types of inverse problems, i.e. Eqs. (4) and (6) together with either (9) or (10), were solved by employing the MFS. The stabilisation/regularization of the inverse BVPs considered was achieved by using several SVD-based regularization methods, such as the TRM (Tikhonov and Arsenin, 1986), the DSVD and the TSVD (Hansen, 1998), while the regularization parameter or the truncation number was chosen according to the DP (Morozov, 1966), GCV criterion (Golub et al., 1979) and Hansen’s LC method (Hansen and O’Leary, 1993). The following major conclusions have been drawn from the present study:

- (i) All three regularization methods (R1)–(R3) provide us with a stable solution of the three-dimensional inverse problems (A) and (B), provided that a suitable criterion for the selection of the regularization parameter is used.
- (ii) For the inverse Cauchy problem (A) in a three-dimensional simply connected domain with a piecewise smooth boundary (e.g. Example 1), an accurate and stable solution is obtained if all three regularization methods (R1)–(R3) are combined with any of the criteria (C1)–(C3), for over-, equally- and under-determined Cauchy data.
- (iii) The inverse BVP (B) in a three-dimensional simply connected domain with a smooth boundary (e.g. Example 2) can be solved, in a stable and accurate manner, provided that:

(i) the TRM and DSVD are combined with any of the criteria (C1)–(C3), or the TSVD is employed together with the DP, when over-prescribed data are available on at least two thirds of the boundary; and (ii) all three regularization methods (R1)–(R3) are combined with either the DP or the LC, when over-prescribed data are available on at least a half of the boundary.

Acknowledgements. Liviu Marin acknowledges the financial support received from the Romanian National Authority for Scientific Research (CNCS–UEFISCDI), project number PN–II–ID–PCE–2011–3–0521.

References

- Aliabadi, M.H., 2002. *The Boundary Element Method. Applications in Solids and Structures. Volume 2.* John Wiley & Sons, London.
- Golub, G.H., Heath, M., Wahba, G., 1979. Generalized cross-validation as a method for choosing a good ridge parameter. *Technometrics* **22**, 1–35.
- Gorzelańczyk, P., Kołodziej, J.A., 2008. Some remarks concerning the shape of the shape contour with application of the method of fundamental solutions to elastic torsion of prismatic rods. *Engineering Analysis with Boundary Elements* **32**, 64–75.
- Hansen, P.C., 1994. Regularization tools: a Matlab package for analysis and solution of discrete ill-posed problems. *Numerical Algorithms* **6**, 1–35.
- Hansen, P.C., 1998. *Rank-Deficient and Discrete Ill-Posed Problems: Numerical Aspects of Linear Inversion.* SIAM, Philadelphia.
- Hansen, P.C., 2007. Regularization tools version 4.0 for Matlab 7.3. *Numerical Algorithms* **46**, 189–194, available at www.netlib.org/numeralgo.
- Hansen, P.C., O’Leary, D.P., 1993. The use of the L-curve in the regularization of discrete ill-posed problems. *SIAM Journal on Scientific Computing* **14**, 1487–503.
- Hon, Y.C., Wei, T., 2004. A fundamental solution method for inverse heat conduction problems. *Engineering Analysis with Boundary Elements* **28**, 489–495.

- Hon, Y.C., Wei, T., 2005. The method of fundamental solutions for solving multidimensional heat conduction problems. *CMES: Computer Modeling in Engineering & Sciences* 13, 219–228.
- Karageorghis, A., Lesnic, D., Marin, L., 2011. A survey of applications of the MFS to inverse problems. *Inverse Problems in Science and Engineering* 19, 309–336.
- Karageorghis, A., Lesnic, D., Marin, L., 2014. The method of fundamental solutions for an inverse boundary value problem in static thermo-elasticity. *Computers & Structures* 135, 32–39.
- Karageorghis, A., Smyrlis, Y.–S., 2007. Matrix decomposition MFS algorithms for elasticity and thermo-elasticity problems in axisymmetric domains. *Journal of Computational and Applied Mathematics* 206, 774–795.
- Kozlov, V.A., Maz'ya, V.G., Fomin, A.V., 2009. Uniqueness of the solution to an inverse thermoelasticity problem. *Computational Mathematics and Mathematical Physics* 49, 525–531.
- Kupradze, V.D., Aleksidze, M.A., 1964. The method of functional equations for the approximate solution of certain boundary value problems. *Computational Mathematics and Mathematical Physics* 4, 82–126.
- Marin, L., 2005a. A meshless method for solving the Cauchy problem in three-dimensional elastostatics. *Computers & Mathematics with Applications* 50, 73–92.
- Marin, L., 2005b. Numerical solution of the Cauchy problem for steady-state heat transfer in two-dimensional functionally graded materials. *International Journal of Solids and Structures* 42, 4338–4351.
- Marin, L., 2005c. A meshless method for the numerical solution of the Cauchy problem associated with three-dimensional Helmholtz-type equations. *Applied Mathematics and Computation* 165, 355–374.
- Marin, L., 2008. The method of fundamental solutions for inverse problems associated with the steady-state heat conduction in the presence of sources. *CMES: Computer Modeling in Engineering & Sciences* 30, 99–122.
- Marin, L., Karageorghis, A., 2013a. The MFS–MPS for two-dimensional steady-state thermoelasticity problems. *Engineering Analysis with Boundary Elements* 37, 1004–1020.

- Marin, L., Karageorghis, A., 2013b. The MFS for the Cauchy problem in two-dimensional steady-state linear thermoelasticity. *International Journal of Solids and Structures* 50, 3387–3398.
- Marin, L., Karageorghis, A., Lesnic, D., 2015. A numerical study of the SVD-MFS solution of inverse boundary value problems in two-dimensional steady-state linear thermoelasticity. *Numerical Methods for Partial Differential Equations* 31, 168–201.
- Marin, L., Lesnic, D., 2004. The method of fundamental solutions for the Cauchy problem in two-dimensional linear elasticity. *International Journal of Solids and Structures* 41, 3425–3438.
- Marin, L., Lesnic, D., 2005a. The method of fundamental solutions for the Cauchy problem associated with two-dimensional Helmholtz-type equations. *Computers & Structures* 83, 267–278.
- Morozov, V.A., 1966. On the solution of functional equations by the method of regularization. *Soviet Mathematics Doklady* 7, 414–417.
- Nowacki, W., 1986. *Thermoelasticity*. Pergamon Press, Oxford.
- Rizzo, J., Shippy, D.J., 1977. An advanced boundary integral equation method for three-dimensional thermoelasticity. *International Journal for Numerical Methods in Engineering* 50, 1753–1768.
- Tikhonov, A.N., Arsenin, V.Y., 1986. *Methods for Solving Ill-Posed Problems*. Nauka, Moscow.

Method	$p_T = p_{\mathbf{u}}$	λ or k	$e_{\Gamma_2}(\mathbf{T})$	$e_{\Gamma_2}(\mathbf{q})$	$e_{\Gamma_2}(\mathbf{u})$	$e_{\Gamma_2}(\mathbf{t})$
TRM-LC	1%	1.90×10^{-3}	1.58×10^{-4}	4.55×10^{-3}	7.43×10^{-5}	7.13×10^{-4}
	3%	8.11×10^{-3}	6.49×10^{-4}	1.80×10^{-2}	2.25×10^{-4}	2.52×10^{-3}
	5%	1.08×10^{-2}	8.27×10^{-4}	2.32×10^{-2}	3.38×10^{-4}	3.19×10^{-3}
TRM-GCV	1%	8.23×10^{-4}	9.64×10^{-5}	2.98×10^{-3}	7.53×10^{-5}	1.15×10^{-3}
	3%	2.08×10^{-3}	2.52×10^{-4}	7.66×10^{-3}	1.87×10^{-4}	1.23×10^{-3}
	5%	3.89×10^{-3}	4.52×10^{-4}	1.34×10^{-2}	3.03×10^{-4}	9.28×10^{-4}
TRM-DP	1%	2.87×10^{-4}	1.49×10^{-4}	3.95×10^{-3}	1.34×10^{-4}	3.39×10^{-3}
	3%	6.61×10^{-4}	2.82×10^{-4}	7.87×10^{-3}	2.38×10^{-4}	4.61×10^{-3}
	5%	9.24×10^{-4}	4.08×10^{-4}	1.18×10^{-2}	3.48×10^{-4}	5.47×10^{-3}
DSVD-LC	1%	3.29×10^{-3}	2.69×10^{-4}	7.29×10^{-3}	7.80×10^{-5}	9.11×10^{-4}
	3%	1.13×10^{-2}	8.12×10^{-4}	2.52×10^{-2}	2.57×10^{-4}	3.38×10^{-3}
	5%	2.08×10^{-2}	1.23×10^{-3}	3.28×10^{-2}	4.05×10^{-4}	5.07×10^{-3}
DSVD-GCV	1%	2.36×10^{-4}	2.52×10^{-4}	6.32×10^{-3}	2.11×10^{-4}	4.55×10^{-3}
	3%	7.61×10^{-4}	5.84×10^{-4}	1.05×10^{-2}	4.67×10^{-4}	6.70×10^{-3}
	5%	1.33×10^{-3}	8.88×10^{-4}	1.46×10^{-2}	7.31×10^{-4}	7.52×10^{-3}
DSVD-DP	1%	1.47×10^{-4}	2.64×10^{-4}	8.67×10^{-3}	2.27×10^{-4}	5.88×10^{-3}
	3%	3.39×10^{-4}	5.82×10^{-4}	1.52×10^{-2}	4.61×10^{-4}	1.15×10^{-2}
	5%	5.59×10^{-4}	8.10×10^{-4}	1.89×10^{-2}	6.08×10^{-4}	1.43×10^{-2}
TSVD-LC	1%	202	1.38×10^{-3}	1.14×10^{-1}	9.27×10^{-4}	3.20×10^{-2}
	3%	202	4.13×10^{-3}	3.42×10^{-1}	2.78×10^{-3}	9.61×10^{-2}
	5%	202	6.89×10^{-3}	5.70×10^{-1}	4.63×10^{-3}	1.60×10^{-1}
TSVD-GCV	1%	61	9.21×10^{-5}	2.96×10^{-3}	1.20×10^{-4}	1.62×10^{-3}
	3%	61	1.82×10^{-4}	6.07×10^{-3}	2.21×10^{-4}	2.09×10^{-3}
	5%	61	2.88×10^{-4}	9.62×10^{-3}	3.39×10^{-4}	2.92×10^{-3}
TSVD-DP	1%	90	7.12×10^{-5}	2.12×10^{-3}	8.90×10^{-5}	1.99×10^{-3}
	3%	83	2.53×10^{-4}	7.24×10^{-3}	1.89×10^{-4}	2.47×10^{-3}
	5%	78	4.40×10^{-4}	1.24×10^{-2}	3.19×10^{-4}	3.99×10^{-3}

Table 1: The values of the regularization parameter, λ or truncation number k , and the corresponding accuracy RMS errors, $e_{\Gamma_2}(\mathbf{T})$, $e_{\Gamma_2}(\mathbf{q})$, $e_{\Gamma_2}(\mathbf{u})$ and $e_{\Gamma_2}(\mathbf{t})$, obtained using the regularization methods (R1)–(R3) with the criteria (C1)–(C3) for various amounts of noise added in the Dirichlet data, i.e. $p_T = p_{\mathbf{u}} \in \{1\%, 3\%, 5\%\}$, for Example 1 with $|\Gamma_1|/|\Gamma_2| = 2$.

Method	$p_T = p_u$	λ or k	$e_{\Gamma_2}(T)$	$e_{\Gamma_2}(q)$	$e_{\Gamma_2}(\mathbf{u})$	$e_{\Gamma_2}(\mathbf{t})$
TRM-LC	1%	3.33×10^{-3}	6.04×10^{-4}	2.12×10^{-2}	4.50×10^{-4}	2.45×10^{-3}
	3%	7.41×10^{-3}	1.07×10^{-3}	3.81×10^{-2}	1.25×10^{-3}	4.05×10^{-3}
	5%	1.00×10^{-2}	1.33×10^{-3}	4.55×10^{-2}	1.99×10^{-3}	4.84×10^{-3}
TRM-GCV	1%	6.04×10^{-4}	4.63×10^{-4}	1.67×10^{-2}	3.97×10^{-4}	1.82×10^{-3}
	3%	1.98×10^{-3}	1.29×10^{-3}	4.57×10^{-2}	1.17×10^{-3}	2.18×10^{-3}
	5%	4.41×10^{-3}	1.85×10^{-3}	6.39×10^{-2}	1.97×10^{-3}	3.15×10^{-3}
TRM-DP	1%	5.73×10^{-4}	4.66×10^{-4}	1.68×10^{-2}	3.98×10^{-4}	1.87×10^{-3}
	3%	1.85×10^{-3}	1.30×10^{-3}	4.58×10^{-2}	1.17×10^{-3}	2.18×10^{-3}
	5%	3.05×10^{-3}	2.02×10^{-3}	6.93×10^{-2}	1.95×10^{-3}	2.78×10^{-3}
DSVD-LC	1%	3.52×10^{-3}	6.12×10^{-4}	2.15×10^{-2}	4.55×10^{-4}	2.54×10^{-3}
	3%	1.23×10^{-2}	1.05×10^{-3}	3.51×10^{-2}	1.31×10^{-3}	5.62×10^{-3}
	5%	2.82×10^{-2}	1.58×10^{-3}	4.43×10^{-2}	2.09×10^{-3}	1.10×10^{-2}
DSVD-GCV	1%	2.05×10^{-4}	8.21×10^{-4}	2.70×10^{-2}	6.48×10^{-4}	6.24×10^{-3}
	3%	6.60×10^{-4}	1.70×10^{-3}	5.59×10^{-2}	1.69×10^{-3}	8.02×10^{-3}
	5%	1.18×10^{-3}	2.50×10^{-3}	7.94×10^{-2}	2.76×10^{-3}	8.36×10^{-3}
DSVD-DP	1%	2.93×10^{-4}	7.39×10^{-4}	2.40×10^{-2}	6.71×10^{-4}	4.93×10^{-3}
	3%	8.00×10^{-4}	1.66×10^{-3}	5.33×10^{-2}	1.77×10^{-3}	6.88×10^{-3}
	5%	1.32×10^{-3}	2.48×10^{-3}	7.73×10^{-2}	2.84×10^{-3}	7.60×10^{-3}
TSVD-LC	1%	49	6.46×10^{-4}	2.09×10^{-2}	4.73×10^{-4}	3.52×10^{-3}
	3%	49	1.37×10^{-3}	4.66×10^{-2}	1.21×10^{-3}	3.57×10^{-3}
	5%	49	2.23×10^{-3}	7.46×10^{-2}	1.98×10^{-3}	3.73×10^{-3}
TSVD-GCV	1%	74	4.95×10^{-4}	1.55×10^{-2}	3.96×10^{-4}	2.20×10^{-3}
	3%	58	1.36×10^{-3}	4.61×10^{-2}	1.17×10^{-3}	2.05×10^{-3}
	5%	33	1.06×10^{-3}	3.02×10^{-2}	2.12×10^{-3}	7.76×10^{-3}
TSVD-DP	1%	74	4.95×10^{-4}	1.55×10^{-2}	3.96×10^{-4}	2.20×10^{-3}
	3%	58	1.36×10^{-3}	4.61×10^{-2}	1.17×10^{-3}	2.05×10^{-3}
	5%	58	2.23×10^{-3}	7.42×10^{-2}	1.94×10^{-3}	2.74×10^{-3}

Table 2: The values of the regularization parameter, λ or truncation number k , and the corresponding accuracy RMS errors, $e_{\Gamma_2}(T)$, $e_{\Gamma_2}(q)$, $e_{\Gamma_2}(\mathbf{u})$ and $e_{\Gamma_2}(\mathbf{t})$, obtained using the regularization methods (R1)–(R3) with the criteria (C1)–(C3) for various amounts of noise added in the Dirichlet data, i.e. $p_T = p_u \in \{1\%, 3\%, 5\%\}$, for Example 1 with $|\Gamma_1|/|\Gamma_2| = 1$.

Method	$p_T = p_{\mathbf{u}}$	λ or k	$e_{\Gamma_2}(\mathbf{T})$	$e_{\Gamma_2}(\mathbf{q})$	$e_{\Gamma_2}(\mathbf{u})$	$e_{\Gamma_2}(\mathbf{t})$
TRM-LC	1%	3.27×10^{-3}	1.16×10^{-3}	3.42×10^{-2}	1.28×10^{-3}	8.04×10^{-3}
	3%	6.09×10^{-3}	3.29×10^{-3}	7.59×10^{-2}	3.65×10^{-3}	2.13×10^{-2}
	5%	8.18×10^{-3}	5.35×10^{-3}	1.25×10^{-1}	5.68×10^{-3}	3.30×10^{-2}
TRM-GCV	1%	6.37×10^{-4}	1.60×10^{-3}	4.72×10^{-2}	1.22×10^{-3}	1.03×10^{-2}
	3%	1.65×10^{-3}	3.86×10^{-3}	1.41×10^{-1}	3.48×10^{-3}	2.14×10^{-2}
	5%	3.92×10^{-3}	5.16×10^{-3}	1.32×10^{-1}	5.98×10^{-3}	3.49×10^{-2}
TRM-DP	1%	1.08×10^{-3}	1.40×10^{-3}	4.48×10^{-2}	1.14×10^{-3}	8.07×10^{-3}
	3%	2.94×10^{-3}	3.26×10^{-3}	9.03×10^{-2}	3.58×10^{-3}	2.06×10^{-2}
	5%	5.74×10^{-3}	5.11×10^{-3}	1.23×10^{-1}	5.92×10^{-3}	3.43×10^{-2}
DSVD-LC	1%	2.98×10^{-3}	1.14×10^{-3}	3.47×10^{-2}	1.25×10^{-3}	7.55×10^{-3}
	3%	1.05×10^{-2}	4.05×10^{-3}	9.50×10^{-2}	3.41×10^{-3}	2.06×10^{-2}
	5%	2.00×10^{-2}	7.75×10^{-3}	1.81×10^{-1}	3.99×10^{-3}	2.48×10^{-2}
DSVD-GCV	1%	1.98×10^{-4}	2.73×10^{-3}	5.37×10^{-2}	1.66×10^{-3}	1.57×10^{-2}
	3%	6.89×10^{-4}	5.49×10^{-3}	1.25×10^{-1}	4.09×10^{-3}	2.64×10^{-2}
	5%	1.14×10^{-3}	7.99×10^{-3}	1.89×10^{-1}	6.46×10^{-3}	3.55×10^{-2}
DSVD-DP	1%	3.96×10^{-4}	2.23×10^{-3}	4.74×10^{-2}	1.54×10^{-3}	1.16×10^{-2}
	3%	1.08×10^{-3}	5.06×10^{-3}	1.17×10^{-1}	4.12×10^{-3}	2.15×10^{-2}
	5%	2.11×10^{-3}	7.32×10^{-3}	1.69×10^{-1}	6.72×10^{-3}	2.97×10^{-2}
TSVD-LC	1%	113	1.01×10^{-2}	1.83×10^{-1}	5.18×10^{-3}	4.92×10^{-2}
	3%	113	3.03×10^{-2}	5.48×10^{-1}	1.55×10^{-2}	1.47×10^{-1}
	5%	117	5.05×10^{-2}	9.14×10^{-1}	2.57×10^{-2}	2.46×10^{-1}
TSVD-GCV	1%	55	1.69×10^{-3}	4.83×10^{-2}	7.46×10^{-3}	9.20×10^{-2}
	3%	49	4.52×10^{-3}	1.49×10^{-1}	3.65×10^{-3}	3.22×10^{-2}
	5%	30	4.85×10^{-3}	1.10×10^{-1}	6.51×10^{-3}	3.89×10^{-2}
TSVD-DP	1%	54	1.53×10^{-3}	5.80×10^{-2}	1.10×10^{-3}	1.04×10^{-2}
	3%	49	4.52×10^{-3}	1.49×10^{-1}	3.65×10^{-3}	3.22×10^{-2}
	5%	47	7.67×10^{-3}	2.43×10^{-1}	6.20×10^{-3}	5.21×10^{-2}

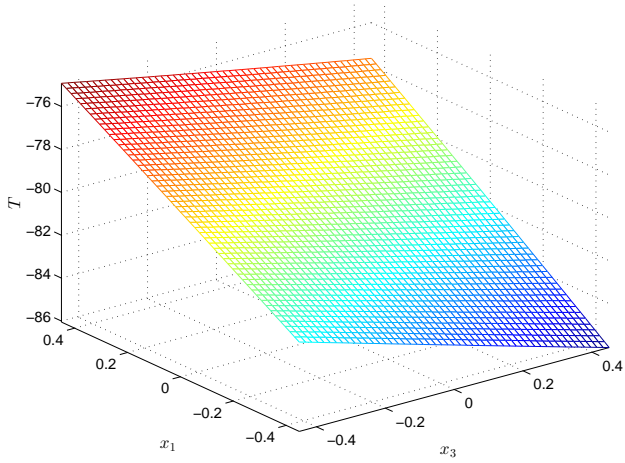
Table 3: The values of the regularization parameter, λ or truncation number k , and the corresponding accuracy RMS errors, $e_{\Gamma_2}(\mathbf{T})$, $e_{\Gamma_2}(\mathbf{q})$, $e_{\Gamma_2}(\mathbf{u})$ and $e_{\Gamma_2}(\mathbf{t})$, obtained using the regularization methods (R1)–(R3) with the criteria (C1)–(C3) for various amounts of noise added in the Dirichlet data, i.e. $p_T = p_{\mathbf{u}} \in \{1\%, 3\%, 5\%\}$, for Example 1 with $|\Gamma_1|/|\Gamma_2| = 1/2$.

Method	$p_T = p_u = p_t$	λ or k	$e_{\Gamma_2}(T)$	$e_{\partial\Omega}(q)$	$e_{\Gamma_2}(\mathbf{u})$
TRM-LC	1%	5.23×10^{-3}	1.47×10^{-3}	5.22×10^{-2}	1.04×10^{-4}
	3%	3.01×10^{-2}	9.34×10^{-3}	2.46×10^{-1}	6.68×10^{-4}
	5%	3.93×10^{-2}	1.05×10^{-2}	2.80×10^{-1}	9.12×10^{-4}
TRM-GCV	1%	1.19×10^{-3}	6.74×10^{-4}	3.07×10^{-2}	5.94×10^{-5}
	3%	2.31×10^{-3}	2.35×10^{-3}	7.33×10^{-2}	2.03×10^{-4}
	5%	3.01×10^{-3}	4.31×10^{-3}	1.13×10^{-1}	3.60×10^{-4}
TRM-DP	1%	2.95×10^{-3}	8.20×10^{-4}	3.62×10^{-2}	7.02×10^{-5}
	3%	8.03×10^{-3}	4.09×10^{-3}	9.91×10^{-2}	2.94×10^{-4}
	5%	1.12×10^{-2}	6.57×10^{-3}	1.49×10^{-1}	4.72×10^{-4}
DSVD-LC	1%	7.79×10^{-3}	2.39×10^{-3}	7.17×10^{-2}	1.56×10^{-4}
	3%	2.97×10^{-2}	9.29×10^{-3}	2.44×10^{-1}	6.62×10^{-4}
	5%	5.47×10^{-2}	1.13×10^{-2}	3.11×10^{-1}	1.37×10^{-3}
DSVD-GCV	1%	2.76×10^{-4}	2.34×10^{-3}	6.19×10^{-2}	1.68×10^{-4}
	3%	8.46×10^{-4}	4.60×10^{-3}	1.24×10^{-1}	4.28×10^{-4}
	5%	1.44×10^{-3}	6.39×10^{-3}	1.70×10^{-1}	6.85×10^{-4}
DSVD-DP	1%	1.08×10^{-3}	1.57×10^{-3}	4.62×10^{-2}	3.81×10^{-4}
	3%	2.95×10^{-3}	3.76×10^{-3}	1.03×10^{-1}	1.04×10^{-3}
	5%	4.86×10^{-3}	5.63×10^{-3}	1.51×10^{-1}	1.71×10^{-3}
TSVD-LC	1%	46	1.18×10^{-2}	3.21×10^{-1}	6.87×10^{-4}
	3%	412	5.49×10^{-2}	1.95×10^0	2.61×10^{-3}
	5%	412	9.15×10^{-2}	3.25×10^0	4.53×10^{-3}
TSVD-GCV	1%	101	8.41×10^2	8.56×10^4	1.69×10^1
	3%	3359	2.52×10^3	2.57×10^5	4.94×10^1
	5%	3359	4.20×10^3	4.28×10^5	8.14×10^1
TSVD-DP	1%	101	7.88×10^{-4}	3.00×10^{-2}	6.73×10^{-5}
	3%	68	2.85×10^{-3}	7.77×10^{-2}	2.23×10^{-4}
	5%	67	1.06×10^{-2}	2.02×10^{-1}	6.96×10^{-4}

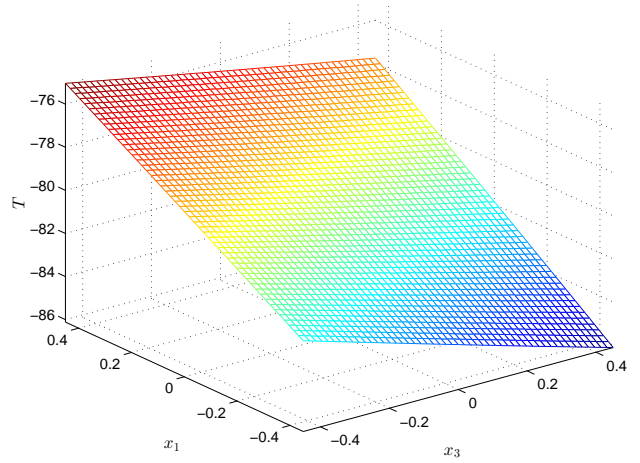
Table 4: The values of the regularization parameter, λ or truncation number k , and the corresponding accuracy RMS errors, $e_{\Gamma_2}(T)$, $e_{\partial\Omega}(q)$ and $e_{\Gamma_2}(\mathbf{u})$, obtained using the regularization methods (R1)–(R3) with the criteria (C1)–(C3) for various amounts of noise added in the boundary data, i.e. $p_T = p_u = p_t \in \{1\%, 3\%, 5\%\}$, for 2 with $|\Gamma_1|/|\Gamma_2| = 2$, i.e. $\phi_0 = 2\pi/3$.

Method	$p_T = p_u = p_t$	λ or k	$e_{\Gamma_2}(T)$	$e_{\partial\Omega}(q)$	$e_{\Gamma_2}(\mathbf{u})$
TRM-LC	1%	4.05×10^{-3}	5.34×10^{-3}	8.65×10^{-2}	4.03×10^{-4}
	3%	2.32×10^{-2}	1.74×10^{-2}	2.92×10^{-1}	1.57×10^{-3}
	5%	2.95×10^{-2}	1.73×10^{-2}	3.08×10^{-1}	2.15×10^{-3}
TRM-GCV	1%	1.10×10^{-5}	8.39×10^{-2}	1.59×10^0	5.04×10^{-3}
	3%	1.10×10^{-5}	2.52×10^{-1}	4.78×10^0	1.51×10^{-2}
	5%	5.83×10^{-3}	9.93×10^{-3}	1.85×10^{-1}	1.24×10^{-3}
TRM-DP	1%	2.82×10^{-3}	3.21×10^{-3}	6.19×10^{-2}	2.93×10^{-4}
	3%	7.68×10^{-3}	1.11×10^{-2}	1.79×10^{-1}	9.48×10^{-4}
	5%	1.27×10^{-2}	1.44×10^{-2}	2.48×10^{-1}	1.43×10^{-3}
DSVD-LC	1%	7.27×10^{-3}	1.02×10^{-2}	1.51×10^{-1}	7.09×10^{-4}
	3%	2.60×10^{-2}	1.78×10^{-2}	3.00×10^{-1}	1.70×10^{-3}
	5%	4.76×10^{-2}	1.86×10^{-2}	3.35×10^{-1}	3.50×10^{-3}
DSVD-GCV	1%	9.33×10^{-6}	8.03×10^{-2}	1.63×10^0	4.71×10^{-3}
	3%	9.33×10^{-6}	2.41×10^{-1}	4.89×10^0	1.41×10^{-2}
	5%	9.33×10^{-6}	4.01×10^{-1}	8.15×10^0	2.36×10^{-2}
DSVD-DP	1%	1.03×10^{-3}	1.42×10^{-3}	5.07×10^{-2}	7.17×10^{-4}
	3%	3.33×10^{-3}	4.14×10^{-3}	1.20×10^{-1}	2.25×10^{-3}
	5%	5.50×10^{-3}	6.06×10^{-3}	1.72×10^{-1}	3.71×10^{-3}
TSVD-LC	1%	93	2.12×10^{-3}	6.09×10^{-2}	2.61×10^{-4}
	3%	58	1.80×10^{-2}	3.33×10^{-1}	1.29×10^{-3}
	5%	58	1.91×10^{-2}	3.38×10^{-1}	1.39×10^{-3}
TSVD-GCV	1%	3359	6.27×10^4	5.16×10^6	1.42×10^3
	3%	3359	1.88×10^5	1.55×10^7	4.25×10^3
	5%	3359	3.13×10^5	2.58×10^7	7.08×10^3
TSVD-DP	1%	104	2.16×10^{-3}	6.03×10^{-2}	2.60×10^{-4}
	3%	67	1.77×10^{-2}	2.47×10^{-1}	1.33×10^{-3}
	5%	67	1.76×10^{-2}	2.68×10^{-1}	1.55×10^{-3}

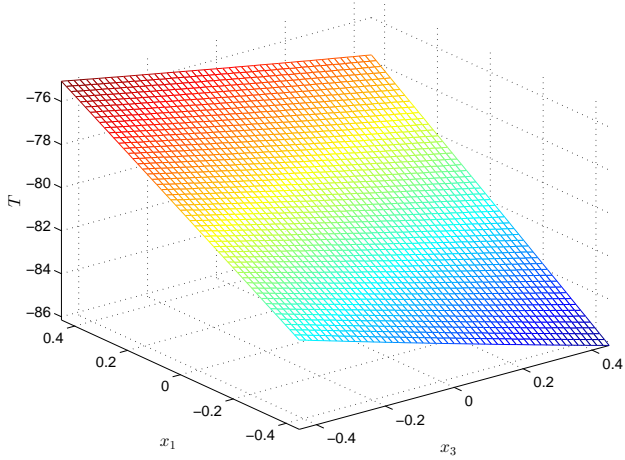
Table 5: The values of the regularization parameter, λ or truncation number k , and the corresponding accuracy RMS errors, $e_{\Gamma_2}(T)$, $e_{\partial\Omega}(q)$ and $e_{\Gamma_2}(\mathbf{u})$, obtained using the regularization methods (R1)–(R3) with the criteria (C1)–(C3) for various amounts of noise added in the boundary data, i.e. $p_T = p_u = p_t \in \{1\%, 3\%, 5\%\}$, for Example 2 with $|\Gamma_1|/|\Gamma_2| = 1$, i.e. $\phi_0 = \pi/2$.



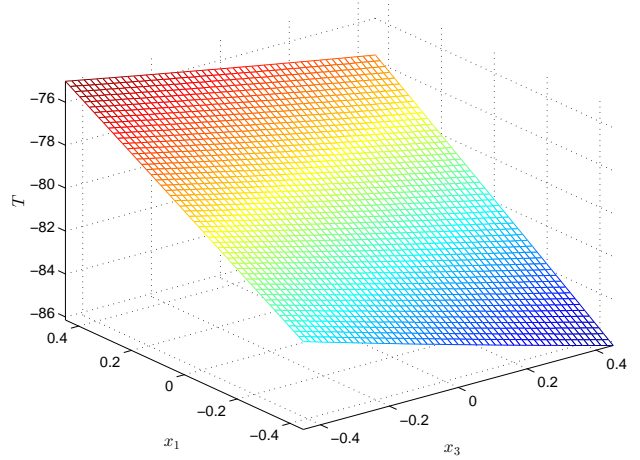
(a) $T^{(\text{an})}|_{x_2=0.5}$



(b) $T^{(\text{num})}|_{x_2=0.5}; p_T = p_u = 1\%$

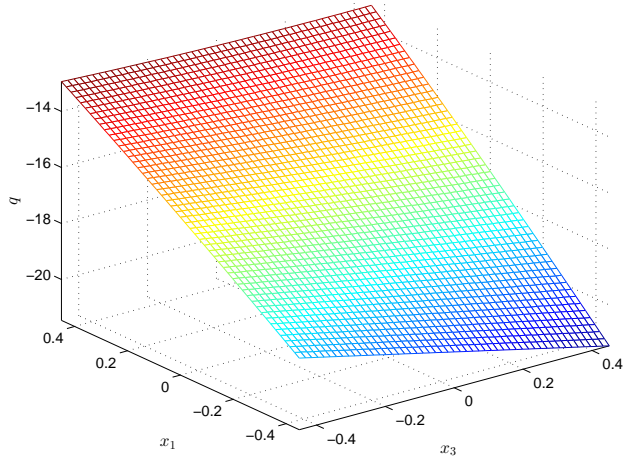


(c) $T^{(\text{num})}|_{x_2=0.5}; p_T = p_u = 3\%$

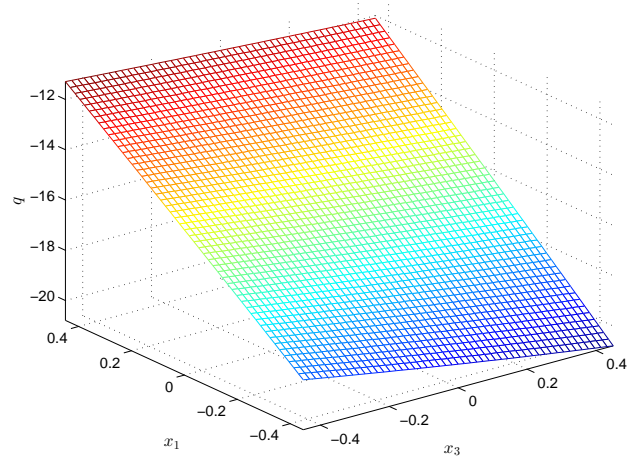


(d) $T^{(\text{num})}|_{x_2=0.5}; p_T = p_u = 5\%$

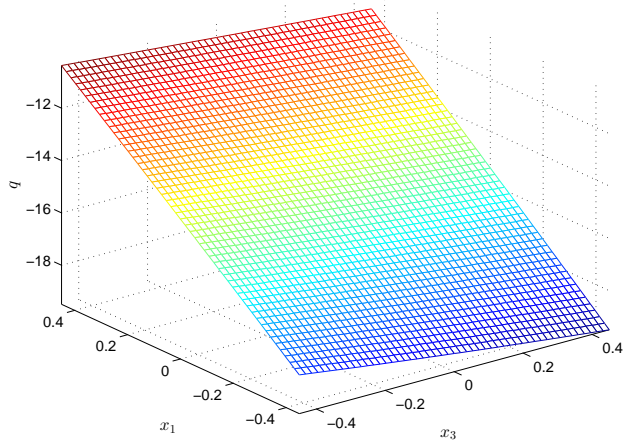
Figure 1: The (a) analytical $T^{(\text{an})}|_{x_2=0.5}$, and (b)–(d) numerical temperatures $T^{(\text{num})}|_{x_2=0.5}$, obtained using the TRM–LC approach and various levels of noise added in $T|_{\Gamma_1}$ and $\mathbf{u}|_{\Gamma_1}$, for Example 1 with $|\Gamma_1|/|\Gamma_2| = 1$.



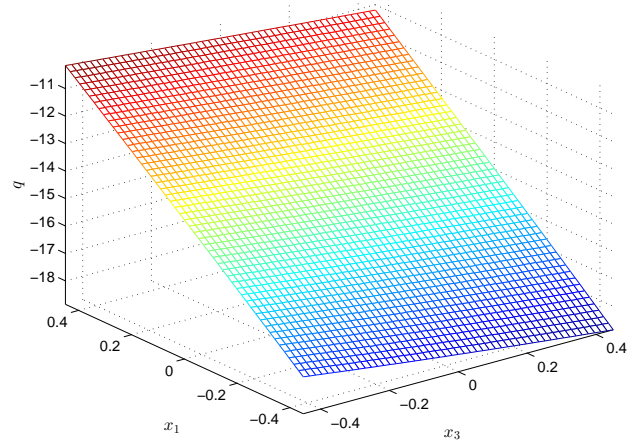
(a) $q^{(\text{an})}|_{x_2=0.5}$



(b) $q^{(\text{num})}|_{x_2=0.5}$: $p_T = p_u = 1\%$



(c) $q^{(\text{num})}|_{x_2=0.5}$: $p_T = p_u = 3\%$



(d) $q^{(\text{num})}|_{x_2=0.5}$: $p_T = p_u = 5\%$

Figure 2: The (a) analytical $q^{(\text{an})}|_{x_2=0.5}$, and (b)–(d) numerical fluxes $q^{(\text{num})}|_{x_2=0.5}$, obtained using the TRM–LC approach and various levels of noise added in $T|_{\Gamma_1}$ and $\mathbf{u}|_{\Gamma_1}$, for Example 1 with $|\Gamma_1|/|\Gamma_2| = 1$.

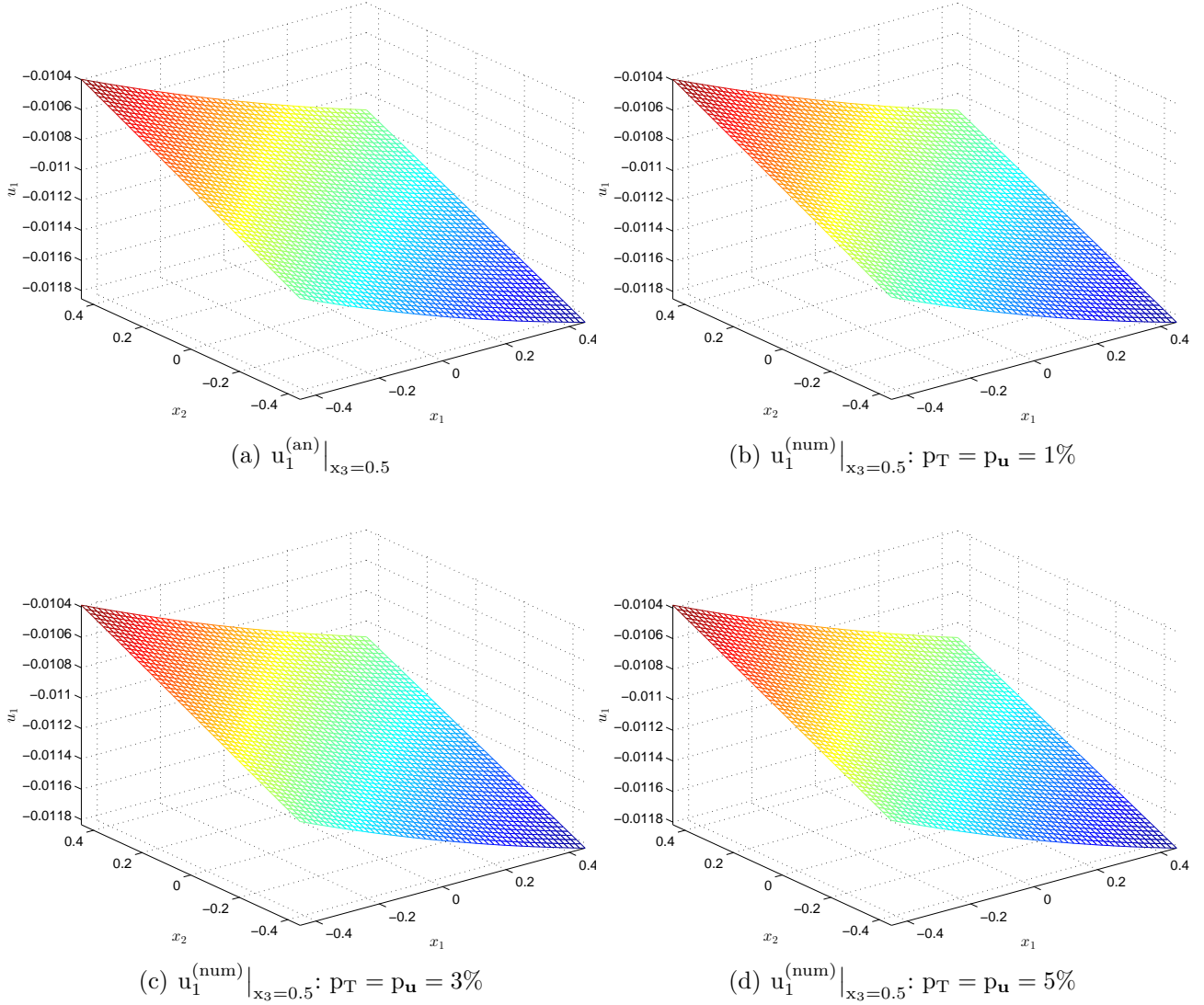


Figure 3: The (a) analytical $u_1^{(\text{an})}|_{x_3=0.5}$, and (b)–(d) numerical displacements $u_1^{(\text{num})}|_{x_3=0.5}$, obtained using the TRM–LC approach and various levels of noise added in $\mathbf{T}|_{\Gamma_1}$ and $\mathbf{u}|_{\Gamma_1}$, for Example 1 with $|\Gamma_1|/|\Gamma_2| = 1$.

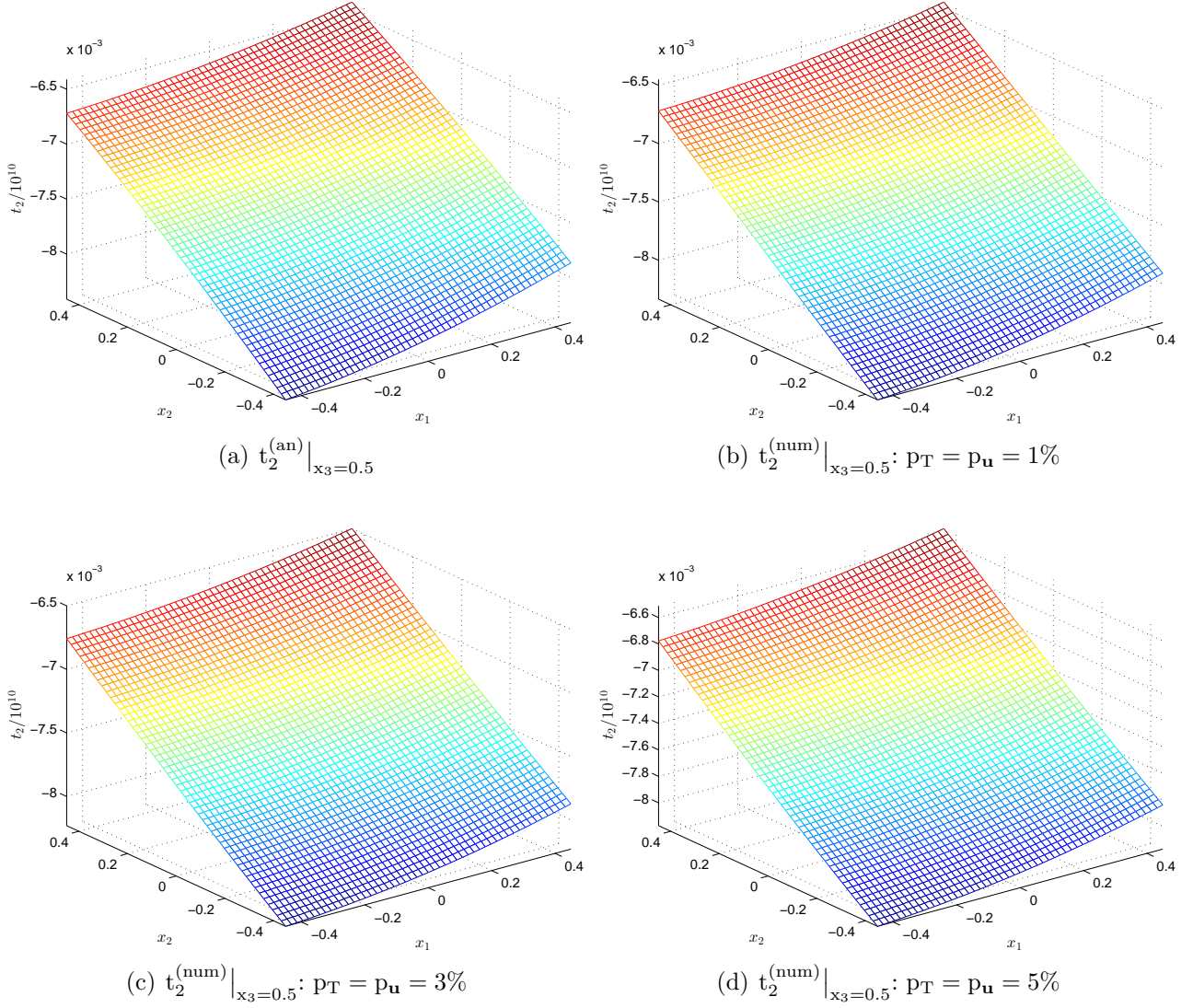
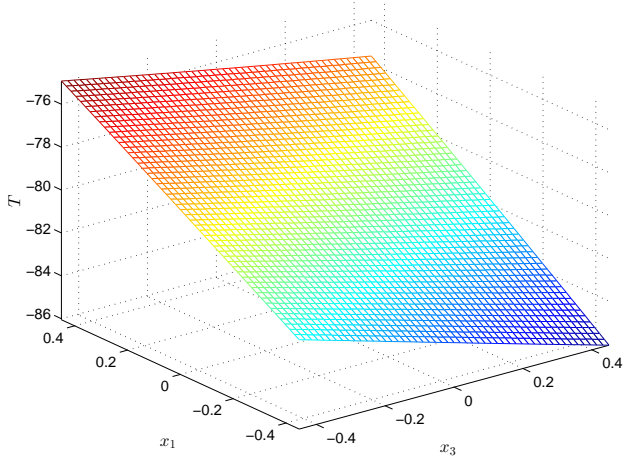
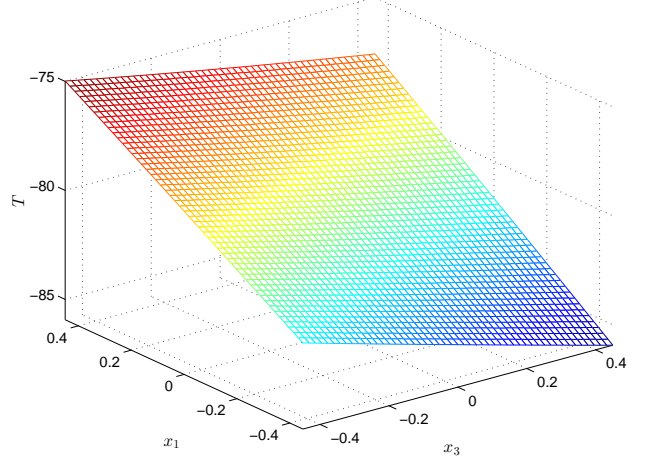


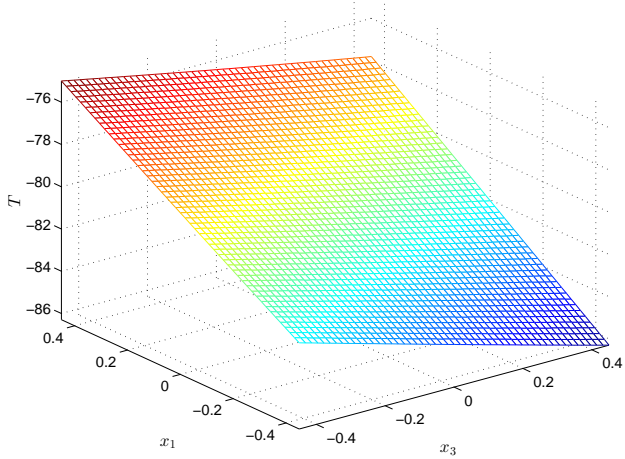
Figure 4: The (a) analytical $t_2^{(\text{an})}|_{x_3=0.5}$, and (b)–(d) numerical tractions $t_2^{(\text{num})}|_{x_3=0.5}$, obtained using the TRM–LC approach and various levels of noise added in $\mathbf{T}|_{\Gamma_1}$ and $\mathbf{u}|_{\Gamma_1}$, for Example 1 with $|\Gamma_1|/|\Gamma_2| = 1$.



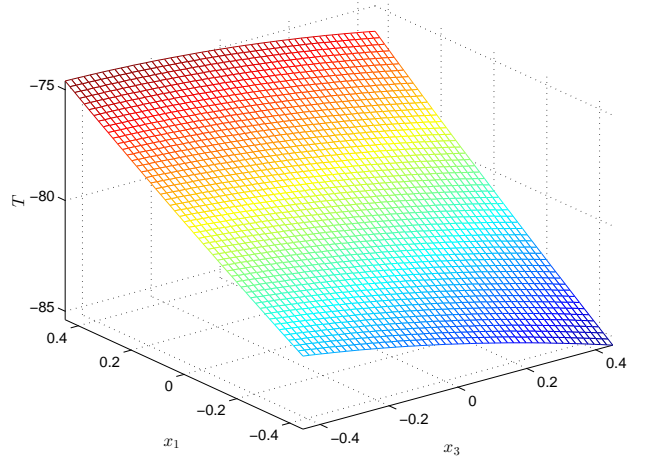
(a) $T^{(\text{an})}|_{x_2=0.5}$



(b) $T^{(\text{num})}|_{x_2=0.5}: |\Gamma_1|/|\Gamma_2| = 2$

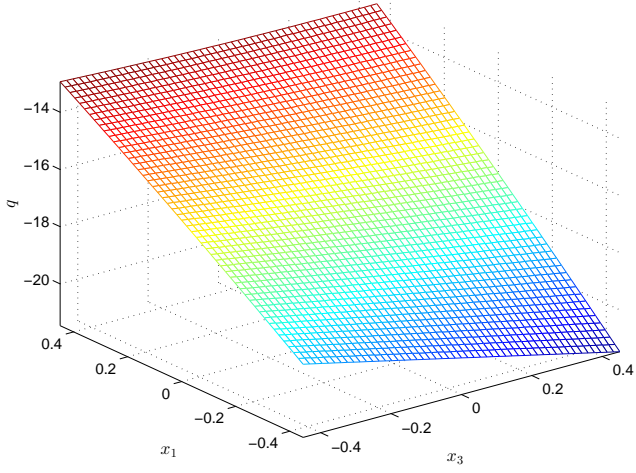


(c) $T^{(\text{num})}|_{x_2=0.5}: |\Gamma_1|/|\Gamma_2| = 1$

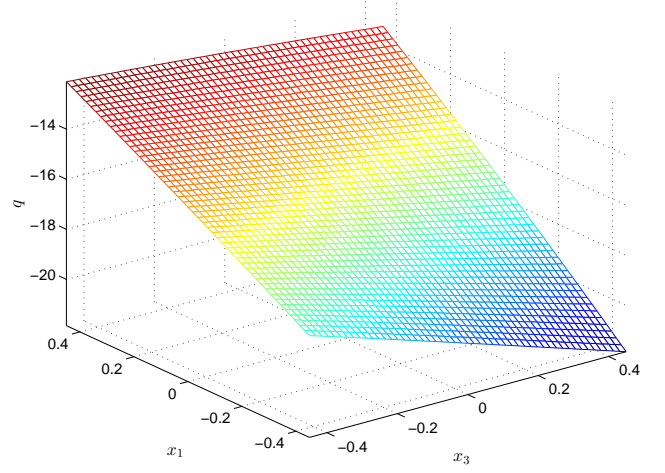


(d) $T^{(\text{num})}|_{x_2=0.5}: |\Gamma_1|/|\Gamma_2| = 1/2$

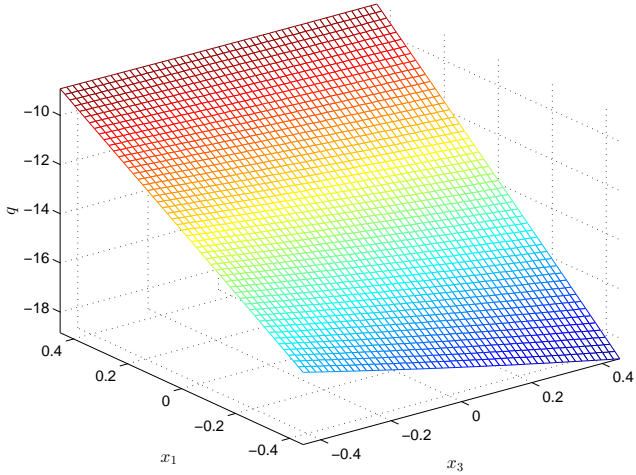
Figure 5: The (a) analytical $T^{(\text{an})}|_{x_2=0.5}$, and numerical temperatures $T^{(\text{num})}|_{x_2=0.5}$, obtained using the TSVD–DP approach and $p_T = p_u = 5\%$, for Example 1 with (b) $|\Gamma_1|/|\Gamma_2| = 2$, (c) $|\Gamma_1|/|\Gamma_2| = 1$, and (d) $|\Gamma_1|/|\Gamma_2| = 1/2$.



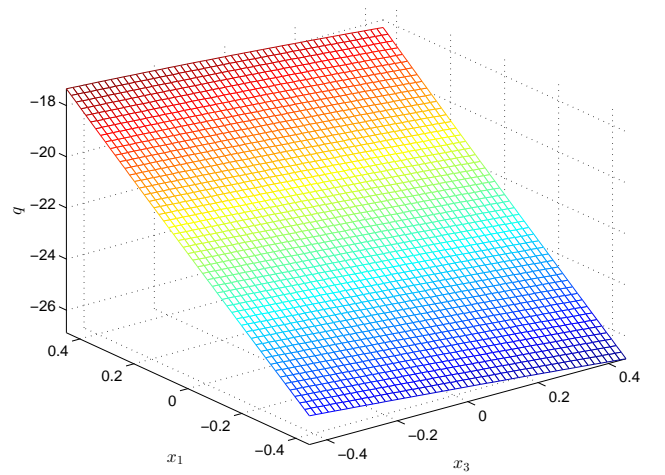
(a) $q^{(\text{an})}|_{x_2=0.5}$



(b) $q^{(\text{num})}|_{x_2=0.5}: |\Gamma_1|/|\Gamma_2| = 2$

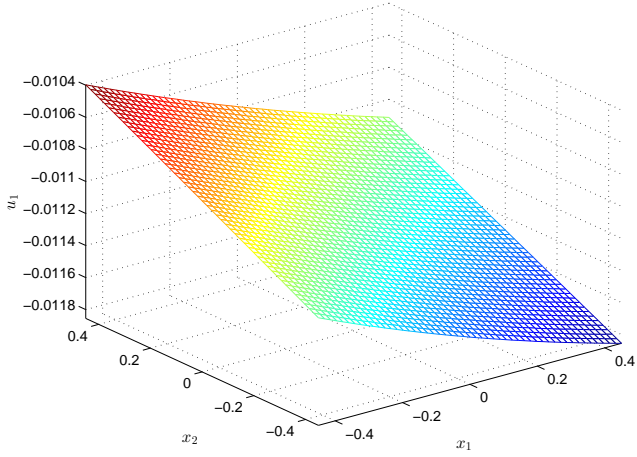


(c) $q^{(\text{num})}|_{x_2=0.5}: |\Gamma_1|/|\Gamma_2| = 1$

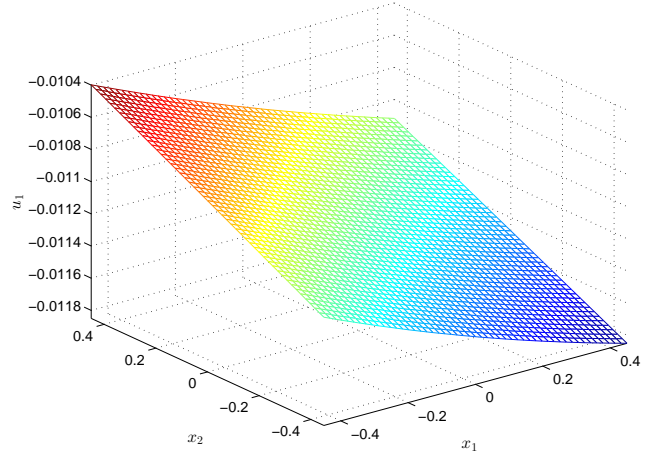


(d) $q^{(\text{num})}|_{x_2=0.5}: |\Gamma_1|/|\Gamma_2| = 1/2$

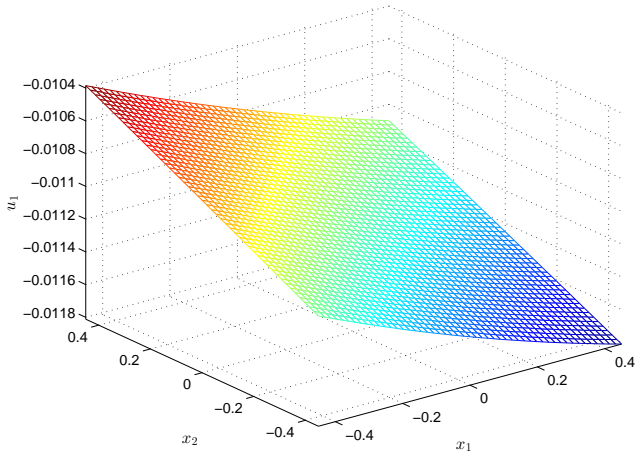
Figure 6: The (a) analytical $q^{(\text{an})}|_{x_2=0.5}$, and numerical normal heat fluxes $q^{(\text{num})}|_{x_2=0.5}$, obtained using the TSVD–DP approach and $p_T = p_u = 5\%$, for Example 1 with (b) $|\Gamma_1|/|\Gamma_2| = 2$, (c) $|\Gamma_1|/|\Gamma_2| = 1$, and (d) $|\Gamma_1|/|\Gamma_2| = 1/2$.



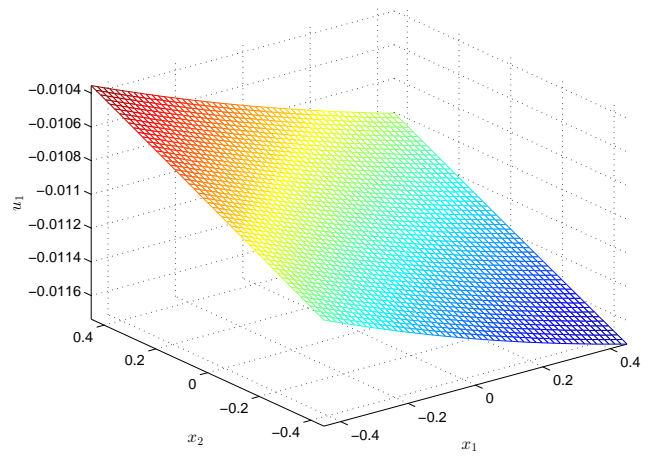
(a) Example 2: $u_1^{(\text{an})}|_{x_3=0.5}$



(b) $u_1^{(\text{num})}|_{x_3=0.5}: |\Gamma_1|/|\Gamma_2| = 2$

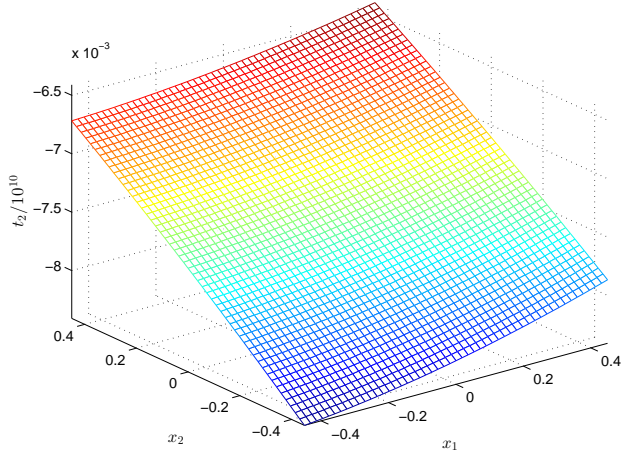


(c) $u_1^{(\text{num})}|_{x_3=0.5}: |\Gamma_1|/|\Gamma_2| = 1$

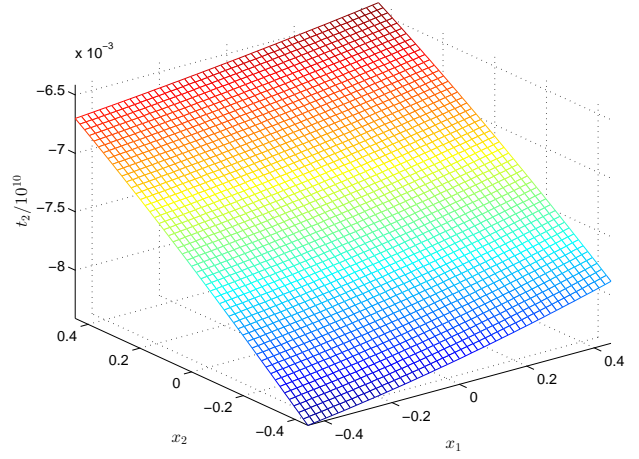


(d) $u_1^{(\text{num})}|_{x_3=0.5}: |\Gamma_1|/|\Gamma_2| = 1/2$

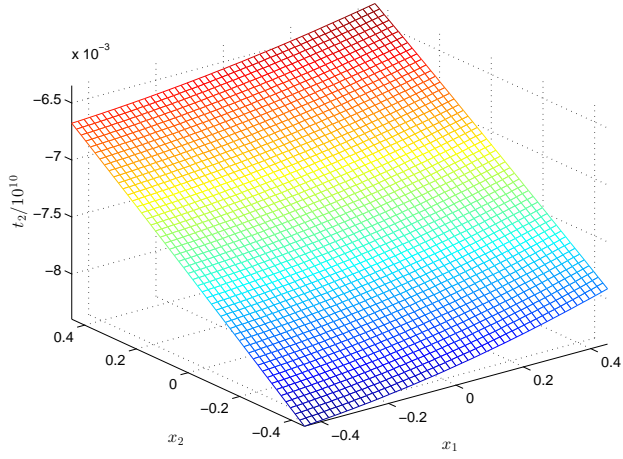
Figure 7: The (a) analytical $u_1^{(\text{an})}|_{x_3=0.5}$, and numerical displacements $u_1^{(\text{num})}|_{x_3=0.5}$, obtained using the TSVD–DP approach and $p_T = p_u = 5\%$, for Example 1 with (b) $|\Gamma_1|/|\Gamma_2| = 2$, (c) $|\Gamma_1|/|\Gamma_2| = 1$, and (d) $|\Gamma_1|/|\Gamma_2| = 1/2$.



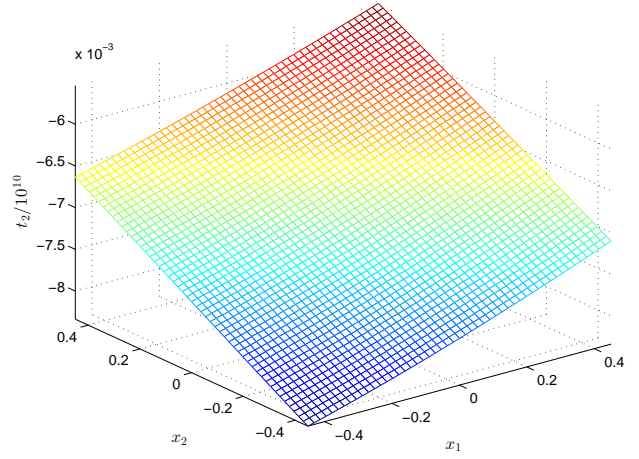
(a) $t_2^{(\text{an})}|_{x_3=0.5}$: Analytical



(b) $t_2^{(\text{num})}|_{x_3=0.5}$: $|\Gamma_1|/|\Gamma_2| = 2$

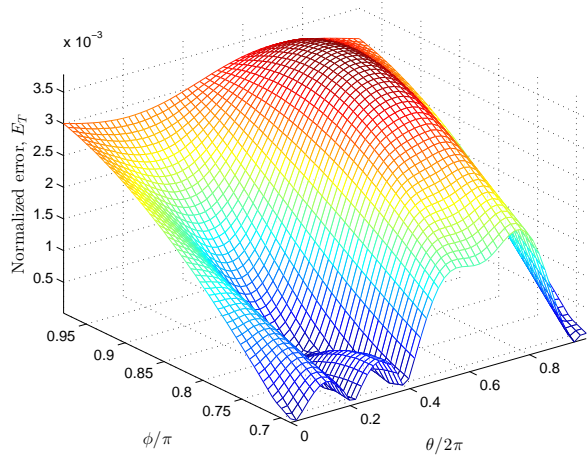


(c) $t_2^{(\text{num})}|_{x_3=0.5}$: $|\Gamma_1|/|\Gamma_2| = 1$

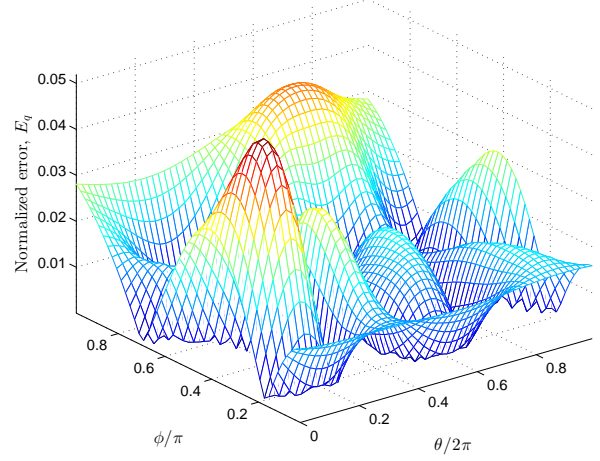


(d) $t_2^{(\text{num})}|_{x_3=0.5}$: $|\Gamma_1|/|\Gamma_2| = 1/2$

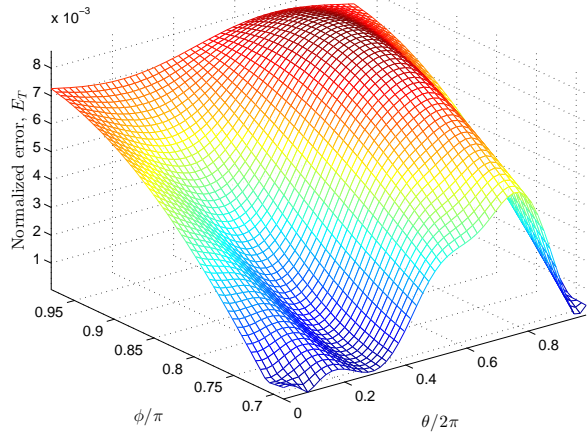
Figure 8: The (a) analytical $t_2^{(\text{an})}|_{x_3=0.5}$, and numerical displacements $t_2^{(\text{num})}|_{x_3=0.5}$, obtained using the TSVD–DP approach and $p_T = p_u = 5\%$, for Example 1 with (b) $|\Gamma_1|/|\Gamma_2| = 2$, (c) $|\Gamma_1|/|\Gamma_2| = 1$, and (d) $|\Gamma_1|/|\Gamma_2| = 1/2$.



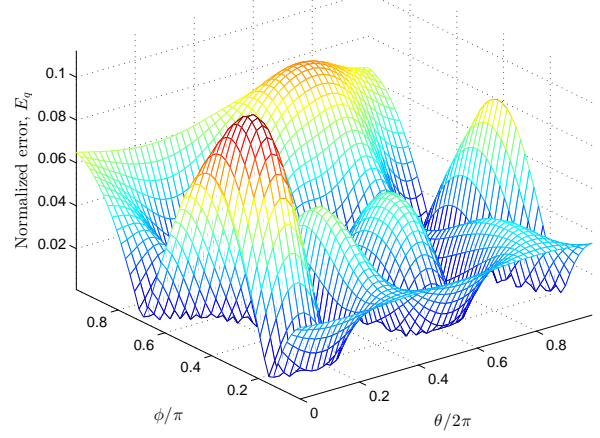
(a) $E_T|_{\Gamma_2}$: $p_T = p_u = p_t = 1\%$



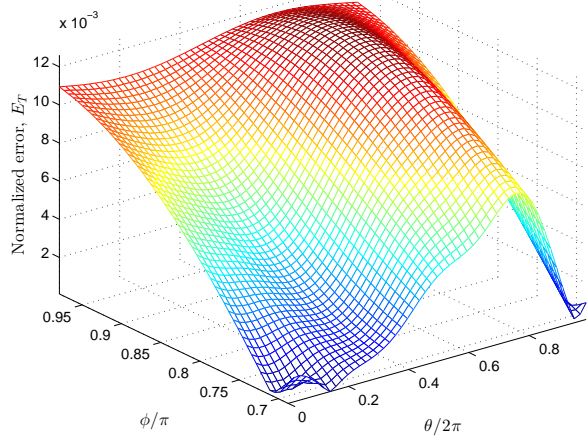
(b) $E_q|_{\partial\Omega}$: $p_T = p_u = p_t = 1\%$



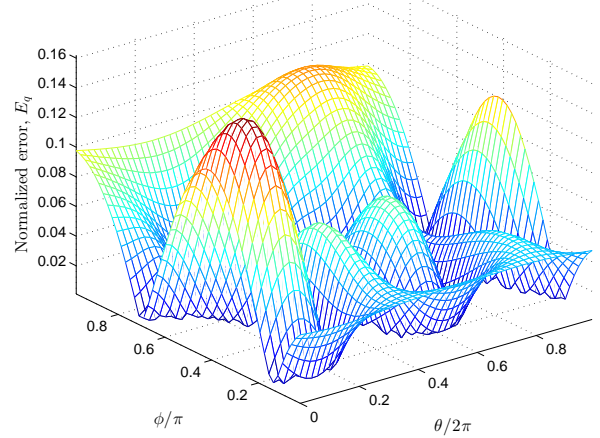
(c) $E_T|_{\Gamma_2}$: $p_T = p_u = p_t = 3\%$



(d) $E_q|_{\partial\Omega}$: $p_T = p_u = p_t = 3\%$

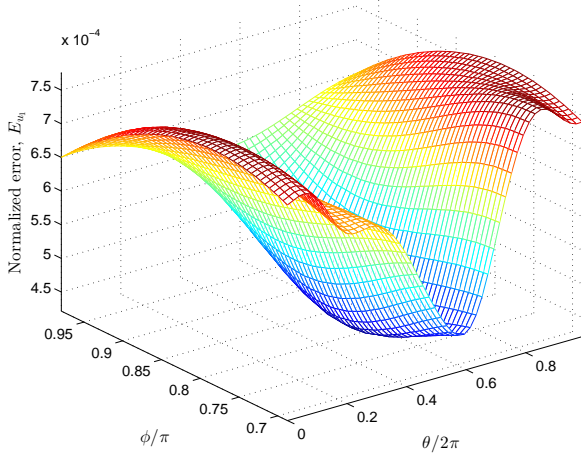


(e) $E_T|_{\Gamma_2}$: $p_T = p_u = p_t = 5\%$

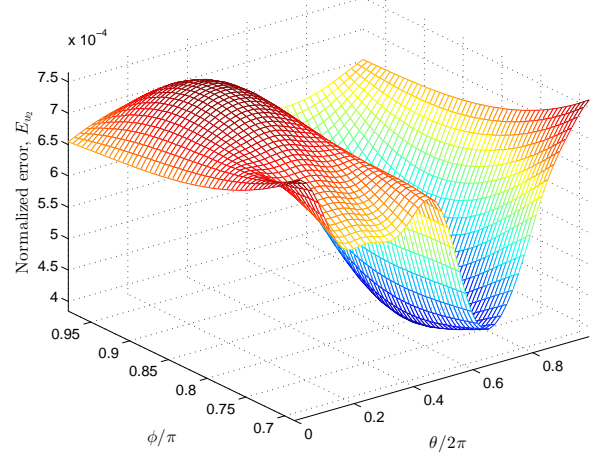


(f) $E_q|_{\partial\Omega}$: $p_T = p_u = p_t = 5\%$

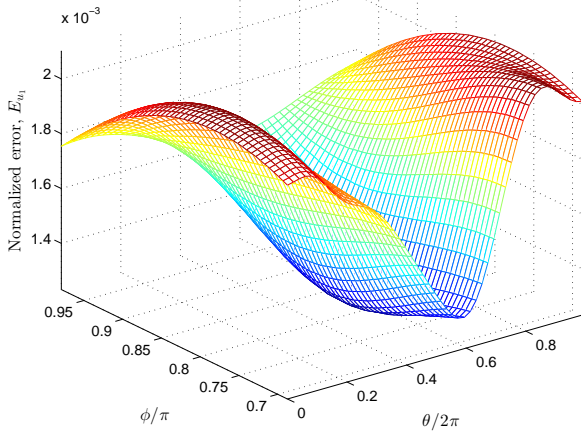
Figure 9: The normalized errors (a), (c) and (e) $E_T|_{\Gamma_2}$, and (b), (d) and (f) $E_q|_{\partial\Omega}$, obtained using the DSVD–DP approach and various levels of noise in $T|_{\Gamma_1}$, $\mathbf{u}|_{\Gamma_1}$ and $\mathbf{t}|_{\partial\Omega}$, for Example 2 with $|\Gamma_1|/|\Gamma_2| = 2$, i.e. $\phi_0 = 2\pi/3$.



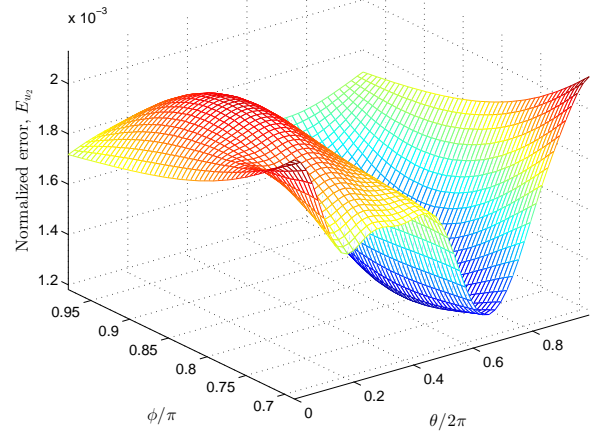
(a) $E_{u_1}|_{\Gamma_2} : p_T = p_u = p_t = 1\%$



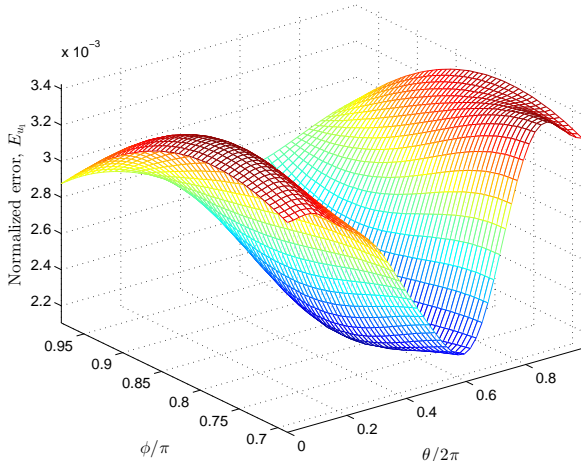
(b) $E_{u_2}|_{\Gamma_2} : p_T = p_u = p_t = 1\%$



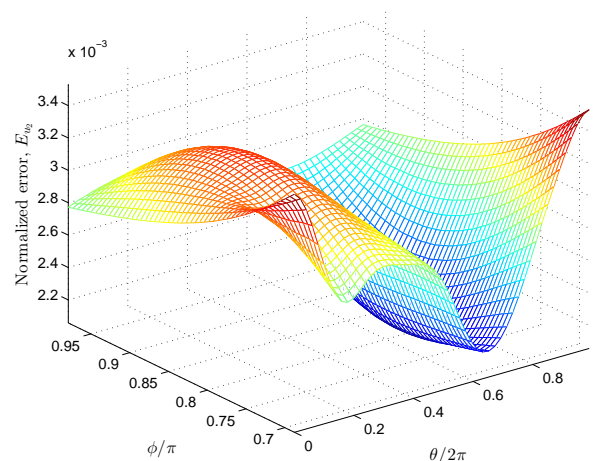
(c) $E_{u_1}|_{\Gamma_2} : p_T = p_u = p_t = 3\%$



(d) $E_{u_2}|_{\Gamma_2} : p_T = p_u = p_t = 3\%$

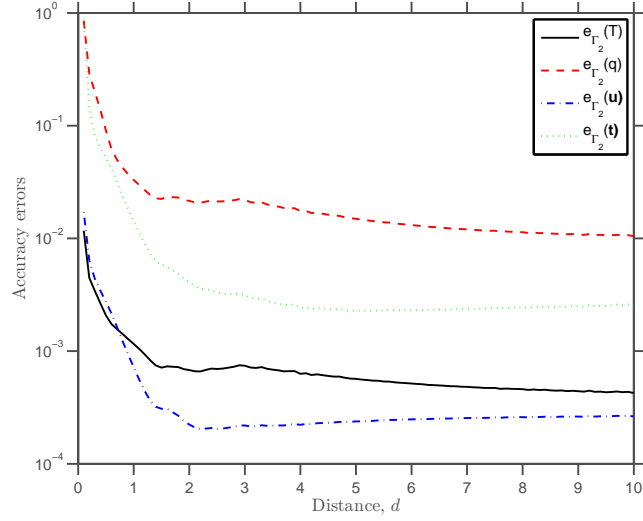


(e) $E_{u_1}|_{\Gamma_2} : p_T = p_u = p_t = 5\%$

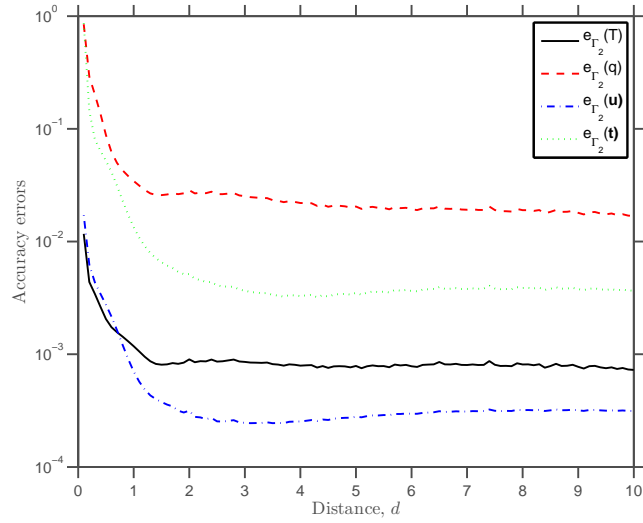


(f) $E_{u_2}|_{\Gamma_2} : p_T = p_u = p_t = 5\%$

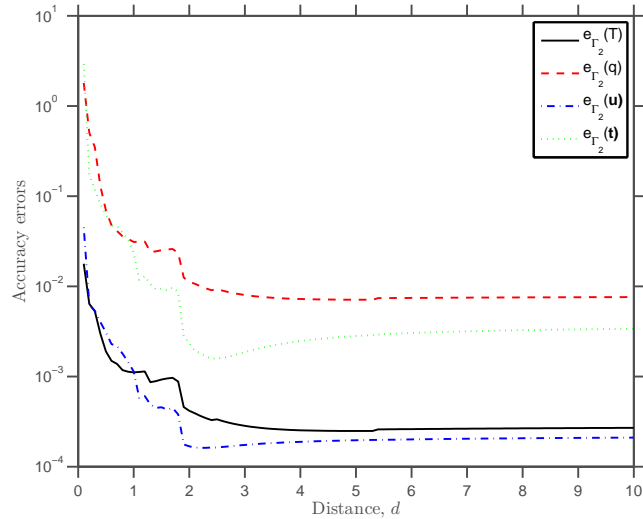
Figure 10: The normalized error (a), (c) and (e) $E_{u_1}|_{\Gamma_2}$, and (b), (d) and (f) $E_{u_2}|_{\Gamma_2}$, obtained using the DSVD–DP approach and various levels of noise in $T|_{\Gamma_1}$, $\mathbf{u}|_{\Gamma_1}$ and $\mathbf{t}|_{\partial\Omega}$, for Example 2 with $|\Gamma_1|/|\Gamma_2| = 2$, i.e. $\phi_0 = 2\pi/3$.



(a) Example 1: TRM-LC



(b) Example 1: DSVD-LC



(c) Example 1: TSVD-DP

Figure 11: The RMS errors $e_{\Gamma_2}(\mathbf{T})$, $e_{\Gamma_2}(\mathbf{q})$, $e_{\Gamma_2}(\mathbf{u})$ and $e_{\Gamma_2}(\mathbf{t})$ as functions of the distance d , obtained using $p_{\mathbf{T}} = p_{\mathbf{u}} = p_{\mathbf{t}} = 3\%$ noise and (a) TRM-LC, (b) DSVD-LC, and (c) TSVD-DP, for Example 1 with $|\Gamma_1|/|\Gamma_2| = 1$.